Multi-year monitoring of atmospheric TGM at a remote high-altitude site (Nam Co, 4730 m a.s.l.) in the inland Tibetan Plateau

Xiufeng Yin [1, 2, 3, 4], Shichang Kang [1, 5], Benjamin de Foy [4], Yaoming Ma [2, 5], Yindong Tong [6], Wei Zhang [7], Xuejun Wang [8], Guoshuai Zhang [2], Qianggong Zhang [2, 5]

[1]State Key Laboratory of Cryospheric Science, Northwest Institute of Eco-Environment and Resources, Chinese Academy of Science, Lanzhou, 730000, China

[2]Key Laboratory of Tibetan Environment Changes and Land Surface Processes, Institute of Tibetan Plateau Research, Chinese Academy of Sciences, Beijing, 100101, China

[3]University of Chinese Academy of Sciences, Beijing, 100039, China

[4]Department of Earth and Atmospheric Sciences, Saint Louis University, St. Louis, MO, 63108, USA

[5]CAS Center for Excellence in Tibetan Plateau Earth Sciences, Beijing, 100101, China

[6]School of Environmental Science and Engineering, Tianjin University, Tianjin, 300072, China

[7]School of Environment and Natural Resources, Renmin University of China, Beijing, 100872, China

[8]College of Urban and Environmental Sciences, Peking University, Beijing, 100871, China

Correspondence to: Qianggong Zhang (qianggong.zhang@itpcas.ac.cn) and Shichang Kang (shichang.kang@lzb.ac.cn)

Abstract

Total gaseous mercury (TGM) concentrations were continuously measured at the Nam Co Station, a remote high-altitude site (4730 m a.s.l.), in the inland Tibetan Plateau, China from January 2012 to October 2014 using a Tekran 2537B instrument. The mean concentration of TGM during the entire monitoring period was 1.33 ± 0.24 ng m^{-3} (mean $\pm$ standard deviation (SD)), ranking the lowest value among all continuous TGM measurements reported all over China, and was lower than most of sites in the Northern Hemisphere. This indicated the pristine atmospheric environment in the inland Tibetan Plateau. Long-term TGM at the Nam Co Station exhibited a slight decrease especially for summer seasons. The seasonal variation of TGM was characterized by higher concentrations during warm seasons and lower concentrations during cold seasons, decreasing in the following order: summer (1.50 ± 0.20 ng m^{-3}) > spring (1.28 ± 0.20 ng m^{-3}) > autumn (1.22 ± 0.17 ng m^{-3}) > winter (1.14 ± 0.18 ng m^{-3}). Diurnal variations of TGM exhibited uniform patterns in different seasons: the daily maximum was reached in the morning (around 2-4 hours after sunrise), followed by a decrease until sunset and a subsequent build-up at night, especially in the summer and the spring. Regional surface re-emission and vertical mixing were two major contributors to the temporal variations of TGM while long-range transported atmospheric mercury promoted elevated TGM during warm seasons. Results of multiple linear regression (MLR) revealed that humidity and temperature were the principal covariates of TGM. Potential source contribution function (PSCF) and FLEXible PARTicle dispersion model (WRF-FLEXPART) results indicated that the likely high potential source regions of TGM to the Nam Co are central and eastern Indo-Gangetic Plain (IGP) during the measurement period with high biomass burning and anthropogenic emissions. The seasonality of TGM at Nam Co was in phase with the Indian Monsoon Index, implying Indian Summer Monsoon as an important driver for transboundary transport of air pollution into the inland Tibetan Plateau. Our results provided atmospheric mercury baseline in the remote inland Tibetan Plateau and serve as new constraint for assessment of Asian mercury emission and pollution.

1 Introduction

Mercury (Hg) is one of the most toxic environmental pollutant because of the easy uptake of its organic forms by biota and the neurological and cardiovascular damage to humans resulting from bioaccumulation (Schroeder and Munthe, 1998). The majority of the mercury released to the environment is emitted into the atmosphere and can be transported from emission sources to deposition sites around the globe. Unlike other metals in the atmosphere, the majority of atmospheric mercury largely exists in the elemental form (Gaseous Elemental Mercury, GEM). The global residence time of GEM is in the range of 0.5-2 years due to its high volatility, low solubility and chemical stability (Schroeder and Munthe, 1998; Shia et al., 1999). It is therefore transported globally over long distances (tens of thousands of kilometers) far from pollution sources. Horowitz et al. (2017) recently reported that the chemical lifetime of tropospheric GEM against oxidation may be much shorter than previously reported: it could be as short as 2.7 months. GEM accounts for more than 95% of TGM (TGM, Total Gaseous Mercury. RGM, Reactive Gaseous Mercury. TGM= GEM + RGM). RGM and Hg-P (particle-bound mercury) compounds make up the remaining fraction of mercury in the atmosphere, and these two compounds have an estimated lifetime ranging from several days to a few weeks. RGM can be expected to be removed near a few tens to a few hundreds of kilometers from their source while Hg-P is likely to be deposited at intermediate distances of hundreds to thousands of kilometers (Schroeder and Munthe, 1998). RGM and Hg-P are generally depicted as local and regional pollutants, and the dry and wet deposition of RGM and Hg-P are much faster than GEM (Schroeder and Munthe, 1998; Lin and Pehkonen, 1999; Lindberg and Stratton, 1998).

East Asia and South Asia are two of the areas in the world with the fastest economic growth and the highest population density. These two areas are known for their heavily polluted air (Nair et al., 2007; Mukherjee et al., 2009), and anthropogenic mercury emissions in these areas are among the world's highest (Pirrone et al., 2010). China is the largest anthropogenic emitter of mercury worldwide with most of the emissions originating from coal combustion and non-ferrous smelting production (AMAP/UNEP, 2013; Pacyna et al, 2008). Geographically, most of China's mercury emissions are located in eastern and central China (Streets et al., 2005; Wu et al., 2016) (Fig. S1). Atmospheric mercury concentrations in Guizhou, one of the most important mercury producing and coal producing regions in China, was reported to be 6.2 - 9.7 ng m^{-3} of TGM in the capital city of Guiyang between 2001- 2009 (Feng et al., 2004; Liu et al., 2011; Fu et al., 2011). Measurements of

atmospheric mercury at background and remote sites in China include the following sites: Wuzhishan (2011-2012), Mt. Changbai (2008-2010), Mt. Waliguan (2007-2008), Mt. Ailao (2011-2012), Shangeri-La (2009-2010) and Mt. Gongga (2005-2006) with concentrations ranging from 1.58 to 3.98 ng m^{-3} (Liu et al., 2016; Fu et al., 2012b; Fu et al., 2012a; Fu et al. 2015; Zhang et al., 2015; Fu et al., 2008). Similarly, South Asia has serious problems of environmental pollution due to elevated mercury emissions (UNEP, 2013), resulting in hazardous mercury levels reported in water, lake sediment and fish samples (Karunasagar et al., 2006; Parvathi et al., 2010; Subramanian, 2004). Anthropogenic mercury emissions in South Asia were mostly in the Indo-Gangetic Plain (IGP) including most of northern and eastern India, the eastern parts of Pakistan, and all of Bangladesh (Fig. S1) all of which have high population density and many industrial centers. Biomass burning is another important source of atmospheric mercury, especially for TGM/GEM (Pirrone et al., 2010), and can lead to high TGM concentration events at sites far from the emissions (de Foy et al., 2012). Plenty of fire hot spots were observed in South Asia and East Asia including the IGP, the Indo-China Peninsula and southeastern China indicating the biomass burning at these areas (Fig. S2), while few biomass burning events were detected in the Tibetan Plateau (Fig. S2).

Located between South Asia and East Asia, the Tibetan Plateau is a vast high-altitude landform featured by remote and pristine environments. There are limited local anthropogenic activities in the Tibetan Plateau and previous studies reported that the atmospheric environment of the Tibetan Plateau remains global background levels (Fu et al., 2012a; Sheng et al., 2013; Xiao et al., 2012). Notably, mercury records from glaciers and lake sediments suggest that the Tibetan Plateau is an important part of the global mercury cycle, acting as both a sink (mercury deposition to snow) and a source (release of mercury from melting ice) (e.g., Kang et al., 2016; Yang et al., 2010; Sun et al., 2017, Sun et al., 2018). Further, it has been increasingly perceived that the inland of Tibetan Plateau can be influenced by trans-boundary air pollution such as black carbon originating from biomass burning in South Asia by crossing the Himalayas (Xia et al., 2011; Cong et al., 2015; Wan et al., 2015; Li et al., 2016). Studies of mercury in precipitation and water vapor evidenced that the Tibetan Plateau is likely sensitive to pollutant input including mercury (Huang et al., 2012; Huang et al., 2013), and the particulate-bound mercury in total suspended particulates was found at high concentrations in Lhasa with an average of 224 pg m^{-3} which was comparable to other cities in China (Huang et al., 2016). A few measurements of atmospheric mercury at sites on the fringes of the Tibetan Plateau reported TGM concentrations in the range of 1.98-3.98 ng m^{-3} (Fu et al., 2012a; Fu et al., 2008; Zhang et al., 2015), which were slightly

99 higher than the northern hemispherical background level, implying possible impact of anthropogenic emissions. In recent years,

100 China and India signed the Minamata Convention and will probably control mercury emissions more strictly (Selin, 2014).

101 Wu et al. (2017) stated that atmospheric mercury emissions from iron and steel production decreased from 35.6 Mg in 2013 to

102 32.7 Mg in 2015, and Pacyna et al. (2010) estimated that total mercury emissions in China would decrease from 635 Mg in

103 2005 to 290–380 Mg in 2020. Burger et al. (2013) estimated that total mercury emissions in India would increase from 310

104 Mg in 2010 to 540 Mg in 2020. In the context of serious mercury pollution and fast changes of regional mercury emission,

105 atmospheric mercury observations at background sites neighboring regions of higher mercury pollution can provide a scientific

106 basis for evaluating the extent of mercury pollution, for determining potential sources of atmospheric mercury and for

107 informing public policy. The Nam Co Station, an inland site in the Tibetan Plateau, is an ideal site to determine the TGM of

108 the inland Tibetan Plateau because it is rarely affected by locally anthropogenic emission of mercury.

109 In this study, high-time resolution TGM was measured at the Nam Co Station from January 2012 to October 2014 and

110 the temporal characteristics of atmospheric mercury were studied. Comparison with meteorological data, Multiple Linear

111 Regression (MLR) and a box model were used to investigate the temporal mercury variations at the Nam Co Station. HYSPLIT

112 (HYbrid Single-Particle Lagrangian Integrated Trajectory), WRF-FLEXPART (FLEXible PARTicle dispersion model) and

113 Potential Source Contribution Function (PSCF) were used to identify potential sources and impacts from long-range transport.

114 The objective of this study is to (1) summarize the levels and temporal characteristics of TGM at a remote site in the inland

115 Tibetan Plateau in a long-term measurement, (2) identify potential source regions of TGM at the Nam Co Station and (3)

116 provide in-situ observational constraint that may contribute to understand changes in Asian mercury pollution.

117 **2 Measurements and Methods**

118 **2.1 Measurement site**

119 The Nam Co comprehensive observation and research station (namely the Nam Co Station, 30°46.44′ N, 90°59.31′ E,

120 and 4730 m a.s.l.) is a remote site between Nam Co Lake and the Nyainqêntanglha mountain range (Fig. 1). The Nam Co

121 Station has been established since 2005 for maintaining a long-term record of the meteorological, ecological, and atmospheric

122 measurements in the Tibetan Plateau (Cong et al., 2007; Li et al., 2007; Kang et al., 2011; Huang et al., 2012; Liu et al., 2015;

123 de Foy et al., 2016b). There are restricted point sources of anthropogenic mercury emissions nearby the Nam Co Station.

124 Dangxiong County is the nearest town on the southern slopes of the Nyainqêntanglha mountain range approximately 60 km

125 south from Nam Co and Dangxiong is about 500 m lower than the Nam Co Station. Nomadism and tourism are the only human

126 activities mostly during summer. Lhasa, the largest city in Tibet, is ~125 km south of the Nam Co Station. There was snow at

127 the Nam Co Station discontinuously from October to March. But due to the strong wind at this period and the flat terrain

128 surrounding the station, the snow did not remain on the ground for more than a few days at a time.

129   TGM measurements were conducted at the Nam Co Station starting on January 15, 2012 until October 4, 2014 (Fig. S3).

130 Field operators checked the instruments and created a monitoring log file each day at the Nam Co Station. Measurements were

131 intermittently interrupted because of equipment maintenance and unstable power supply due to damage from strong winds to

132 the electrical wires at the Nam Co Station. All data displayed in this study are in UTC+8 and solar noon at the Nam Co Station

133 is at 13:56 in UTC+8 (China Standard Time, Beijing Time).

134   **2.2 Measurements: TGM, surface ozone and meteorology**

135   Measurements of TGM concentrations were performed with a Tekran model 2537 B instrument (Tekran Instruments

136 Corp., Toronto, Ontario, Canada). The Tekran 2537 B was installed in the monitoring house at the Nam Co Station and ambient

137 air was introduced from the inlet which was 1.5 m above the roof and 4 m above the ground. A 45-mm diameter Teflon filter

138 (pore size 0.2 μm) was placed in front of the inlet and it was changed every two weeks. The Tekran 2537 B measurements are

139 based on the amalgamation of mercury onto a pure gold surface. By using a dual cartridge design, continuous measurements

140 of mercury in the air can be made. The amalgamated mercury was thermally desorbed into an argon carrier gas stream and

141 analyzed using an internal detector which was designed by cold vapor atomic fluorescence spectrophotometry (λ=253.7nm)

142 (Landis et al., 2002) providing TGM analysis at sub-ng m^{-3} levels. The sampling interval of the Tekran 2537 B was 5 min and

143 the sampling flow rate was 0.8 L min^{-1} (at standard temperature and pressure). The Tekran 2537 B was calibrated automatically

144 every 25 hours using the internal mercury permeation source and was calibrated manually using a Tekran 2505 randomly 1-2

145 times a year. At the Nam Co Station, the TGM fraction consists mostly of GEM (more than 98%). The operationally defined

146 RGM accounted for less than 2% of TGM (Figure S1 in supplementary material in de Foy et al., 2016b). We consider the

147 Tekran data to represent TGM in line with previous studies (e.g. Kock et al., 2005; Slemr et al., 2008; Müller et al., 2012).

148 Surface ozone was measured as a surrogate measure of oxidizing potential of the atmosphere (Stamenkovic et al., 2007)

149 at the Nam Co Station using a UV photometric instrument (Thermo Environmental Instruments, USA, Model 49i) which uses

150 absorption of radiation at 254 nm and has a dual cell design. The monitor was calibrated using a 49i-PS calibrator (Thermo

151 Environmental Instruments, USA) before measurements and using aperiodic calibration during the monitoring periods. Details

152 and analysis of the surface ozone measurements at the Nam Co Station were reported in Yin et al. (2017).

153 Measurements of temperature (T), relative humidity (RH), wind speed (WS), wind direction (WD) and downward

154 shortwave radiation (SWD) were conducted at the Nam Co Station by a local weather station system (Milos 520, Vaisala Co.,

155 Finland) and a radiation measurement system (CNR1, Kipp & Zonen Co., US), respectively (Ma et al., 2008).

156 **2.3 Meteorological simulations**

157 Gridded meteorological data for backward trajectories were obtained from the Global Data Assimilation System (GDAS-

158 1) of the U.S. National Oceanic and Atmospheric Administration (NOAA) with 1°×1° latitude and longitude horizontal

159 resolution and vertical levels of 23 from 1000 hPa to 20 hPa (http: // www. arl. noaa. gov/ gdas1. php).

160 Backward trajectories and clusters were calculated using the NOAA-HYSPLIT model (Draxler and Rolph, 2003,

161 http://ready.arl.noaa.gov/HYSPLIT.php) using TrajStat (Wang et al., 2009), which is a free software plugin of MeteoInfo

162 (Wang, 2014). The backward trajectories arrival height in HYSPLIT was set at 500 m above the surface and the total run times

163 was 120 hours for each backward trajectory. Results of air masses at different heights (500m, 1000m and 1500m) showed

164 similar patterns, hence, we selected trajectories released at a height of 500 m as representative since 500 m is suitable for

165 considerations of both the long-range transport and transport in the planetary boundary layer. Trajectory positions were stored

166 at time intervals of 3 hours. Angular distance was chosen to calculate clusters in HYSPLIT calculation. HYSPLIT backward

167 trajectories were used to calculate the Potential Source Contribution Function (section 2.6) which serves to investigate the

168 potential sources contributing to atmospheric mercury at the Nam Co Station.

169 In addition to HYSPLIT, WRF-FLEXPART (Brioude et al., 2013) was used to obtain clusters of particle trajectories

170 reaching the Nam Co Station. 1000 particles were released per hour in the bottom 100 m surface layer above the Nam Co

171 Station and were tracked in backward mode for 4 days (de Foy et al., 2016b). The use of two different trajectory models

172 (HYSPLIT and WRF-FLEXPART) with different input meteorology can add robustness to the discussion as was done for the

173 ozone study at Nam Co (Yin et al., 2017). Furthermore, the WRF-FLEXPART simulations were some of the parameters used

174 in the multiple linear regression model (section 2.4). Residence Time Analysis (RTA) (Ashbaugh et al., 1985) was utilized to

175 show the dominant transport paths of air masses impacting the samples (Wang et al., 2016; Wang et al., 2017). Six clusters

176 were found to represent the prevailing flow patterns to the Nam Co Station simulated using WRF-FLEXPART.

2.4 Multiple linear regression model and box model

178   A Multiple Linear Regression (MLR) model was used to quantify the main factors affecting the hourly concentrations of

179 TGM. The method follows the description provided in de Foy et al. (2016a; 2016c) and de Foy (2017) and was used to analyze

180 surface ozone concentrations at the Nam Co Station (Yin et al., 2017). The inputs to the MLR model include meteorological

181 parameters (wind speed, temperature, solar radiation and humidity), surface ozone, inter-annual variation factors, seasonal

182 factors, diurnal factors, WRF boundary layer heights, WRF-FLEXPART trajectory clusters and a CAMx stratospheric ozone

183 tracer (see Yin et al. (2017) for more details). Briefly, the inter-annual factors are separate scaling factors for each year of the

184 measurements, the seasonal factors are 12-month and 6-month harmonic terms (sine and cosine), and the diurnal factors are

185 scaling factors for each hour of the day. The inputs to the model were normalized linearly. An Iteratively Reweighted Least

186 Squares (IRLS) procedure was used to screen for outliers. Measurement times when the model residual was greater than two

187 standard deviations of all the residuals were excluded from the analysis. This was repeated iteratively until the method

188 converged on a stable set of outliers. The variables to be included in the regression were obtained iteratively. At each iteration,

189 the variable leading to the greatest increase in the square of Pearson's correlation coefficient was added to the inputs as long

190 as the increase was greater than 0.005.

191   The distribution of TGM concentrations is approximately normal (see details in section 3.1), and so a linear model was

192 used. TGM was scaled linearly to have a mean of 0 and a standard deviation of 1 in the regression model. A Kolmogorov-

193 Zurbenko filter (Rao et al., 1997) was used to separate the time series of specific humidity and temperature into a synoptic

scale signal (> 3-5 days) and a diurnal scale signal using 5 passes of a 13-point moving average. Only the synoptic scale signal was included in the final regression results, as the diurnal variation was characterized by the other variables in the analysis. The other meteorological parameters used were the 24-hour average boundary layer height from WRF and the 8-hour local measured wind speeds (4 directions, 5 wind speed segments for a total of 20 factors corresponding to different wind speeds from different wind directions). The 24-hour average of ozone measurements (log-transformed) contributed to the model. In addition, a seasonal K-Z filtered time series of a CAMx tracer for transport from the free troposphere (above 300 hPa) to the surface contributed to the model.

TGM at the Nam Co Station is expected to be well mixed and the site is not influenced by local sources. It is therefore expected that a box model should be able to reproduce the diurnal profile of concentrations. A box model that accurately simulates the diurnal profile of TGM would provide constraints on known processes affecting the concentrations. Comparisons with measured profiles would further identify missing processes in the model. This approach was used for reactive mercury at the same site, where it identified the role of the reduction of reactive mercury to gaseous elementary mercury mediated by sunlight (de Foy et al., 2016b). A box model was made that included free parameters to represent known chemical reactions and dispersion processes. An optimization algorithm was used to identify the parameters required to fit the model to the data, as was done in de Foy et al. (2016b). Preliminary tests of the box model were made using solar radiation and temperature to represent chemical transformations, as well as using wind speed and boundary layer height to represent dilution. However these attempts failed to reproduce the diurnal variation found in the measurements. A simplified exploratory model was therefore sought that would represent the measured diurnal variations as simply as possible, according to Occam's razor (Larsen et al., 2014). Although this model does not yield direct information on known processes, it does identify the kinds of processes and their magnitude that would be required to accurately represent the measured diurnal profile. The final model combined the following 5 inputs: TGM increases at sunrise and in the early evening, constant TGM reductions 24 hours a day, a constant lifetime for TGM loss during daylight hours and TGM dilution due to vertical mixing.

2.5 Anthropogenic mercury emissions and fire hot spots distribution

The mercury emission inventory of China was obtained from Wu et al. (2016), which used a technology-based approach to compile a comprehensive estimate of Chinese provincial emissions for all primary anthropogenic sources. The emissions

219   over other Asian countries were from UNEP global anthropogenic emission inventory (AMAP/UNEP, 2013). These

220   inventories were for the year 2010 and had a horizontal resolution of $0.5°\times0.5°$.

221   MODIS fire spots were obtained from Fire Information for Resource Management System (FIRMS) operated by the

222   National Aeronautics and Space Administration (NASA) of the United States (Giglio et al., 2003; Davies et al., 2004).

223   **2.6 Potential Source Contribution Function (PSCF)**

224   PSCF assumes that back-trajectories arriving at times of higher mixing ratios likely point to the more significant source

225   directions (Ashbaugh et al., 1985). PSCF has been applied in previous studies to locate sources of TGM for different sites (Fu

226   et al., 2012a; Fu et al., 2012b; Zhang et al., 2015). The PSCF values for the grid cells in the study domain are based on a count

227   of the trajectory segment (hourly trajectory positions) that terminate within each cell (Ashbaugh et al., 1985). Let n_{ij} be the

228   total number of endpoints that fall in the ijth cell during whole simulation period. Let m_{ij} represents the number of points in

229   the same cell that have arrival times at the sampling site corresponding to TGM concentrations higher than a set criterion. In

230   this study, we calculate the PSCF based on trajectories corresponding to concentrations that exceed the mean level (1.33 ng m^{-}

231   ^{3}) of TGM. The PSCF value for the ijth cell is then defined as:

232      $PSCF_{ij} = m_{ij}/n_{ij}$

233   The PSCF value can be interpreted as the conditional probability that the TGM concentration at measurement site is

234   greater than the mean mixing ratios if the air parcel passes though the ijth cell before arriving at the measurement site. In cells

235   with high PSCF values are associated with the arrival of air parcels at the receptor site that have TGM concentrations that

236   exceed the criterion value. These cells are indicative of areas of 'high potential' contributions for the chemical constituent.

237   Identical $PSCF_{ij}$ values can be obtained from cells with very different counts of back-trajectory points (e.g. grid cell A

238   with mij=5000 and nij=10000 and grid cell B with mij = 5 and nij = 10). In this extreme situation grid cell A has 1000 times

239   more air parcels passing through than grid cell B. Because of the sparse particle count in grid cell B, the PSCF values are more

240   uncertain and the contribution from B is limited. To account for the uncertainty due to low values of nij, the PSCF values were

241   scaled by a weighting function W_{ij} (Polissar et al., 1999). The weighting function reduced the PSCF values when the total

242   number of the endpoints in a cell was less than about three times the average value of the end points per each cell. In this case,

243   W_{ij} was set as follows:

244   $$W_{ij} = \begin{cases} 1.00 & n_{ij} > 3N_{ave} \\ 0.70 & 3N_{ave} > n_{ij} > 1.5N_{ave} \\ 0.42 & 1.5N_{ave} > n_{ij} > N_{ave} \\ 0.05 & N_{ave} > n_{ij} \end{cases}$$ (1)

245   where N_{ave} represents the mean n_{ij} of all grid cells. The weighted PSCF values obtained by multiplying the original PSCF

246   values by the weighting factor: weighted PSCF result=W_{ij}×PSCF.

247   **3 Results and discussion**

248   **3.1 TGM concentrations**

249   The mean TGM concentration at the Nam Co Station is 1.33±0.24 ng m^{-3}, which is the lowest among all reported TGM

250   concentrations at remote and rural sites in China (Liu et al., 2016; Fu et al., 2012b; Fu et al., 2012a; Fu et al. 2015; Ci et al.,

251   2011; Dou et al., 2013; Zhang et al., 2015; Fu et al., 2010; Li et al., 2011; Zhang et al., 2013; Yu et al., 2015; Fu et al., 2008;

252   Chen et al., 2013). The mean concentration of TGM is slightly lower than the annual mean concentration at background sites

253   in the Northern Hemisphere (1.55 ng m^{-3} in 2013 and 1.51 ng m^{-3} in 2014), and higher than those in the Southern Hemisphere

254   (0.93 ng m^{-3} in 2013 and 0.97 ng m^{-3} in 2014) (Sprovieri et al., 2016). Comparable results were reported from EvK2CNR on

255   the south slope of the Himalayas (1.2 ng m^{-3}, Gratz et al., 2013), and from tropical sites in the Global Mercury Observation

256   System in the Northern Hemisphere (1.23 ng m^{-3} in 2013 and 1.22 ng m^{-3} in 2014) (Sprovieri et al., 2016). Comparing to the

257   three sites at the edge of the Tibetan Plateau (Mt. Waliguan, Shangri-La and Mt. Gongga, Table S1), the mean TGM

258   concentration at the Nam Co Station was substantially lower, indicating that the inland Tibetan Plateau has a more pristine

259   environment than the edges of the plateau.

260   The frequency distribution of TGM at the Nam Co Station was normally distributed (Fig. S4). 81% of hourly average

261   TGM concentrations were in the range of 1.0-1.6 ng m^{-3} with few episodically elevated TGM and low TGM concentrations.

262   1.6% (n=236) out of all hourly mean TGM data (n=14408) were greater than 1.81 ng m^{-3} (overall mean TGM + 2×SD, namely

263   1.33+2×0.24=1.81), and 1.5% (n=213) were lower than 0.85 ng m^{-3} (overall mean TGM - 2×SD, namely 1.33-2×0.24=0.85).

264   The monthly average TGM at the Nam Co Station showed a weak decrease (slope = -0.006) during the entire monitoring

265   period, and the decrease was more pronounced in the summer (slope = -0.013). Despite the short time span of the TGM time

266   series with some missing data mostly in the winter, the slight decrease of TGM especially in the summer was in agreement

267   with a recent study using plant biomonitoring which identified a decreasing atmospheric mercury since 2010 near Dangxiong

268   county (Tong et al., 2016) as well as decreases of TGM at other sites (Slemr et al., 2011; Zhang et al., 2016).

269   **3.2 Seasonal variations of TGM**

270   In contrast with many previous observations in China (Zhang et al., 2015; Fu et al., 2008b; Fu et al., 2009; Fu et al., 2010;

271   Fu et al., 2011; Fu et al., 2012b; Feng et al., 2004; Xiu et al., 2009; Xu et al., 2015; Wan et al., 2009) and most AMNet

272   (Atmospheric Mercury Network) sites (Lan et al., 2012) , TGM at the Nam Co Station showed a seasonal variation with a

273   maximum in the summer (June, July and August) and a minimum in the winter (December, January and February) (Fig. 2).

274   The seasonal mean TGM values decreased in the following order: summer (1.50 ± 0.20 ng m^{-3}) > spring (1.28 ± 0.20 ng m^{-3}) >

275   autumn (1.22 ± 0.17 ng m^{-3}) > winter (1.14 ± 0.18 ng m^{-3}) (Table 1). The highest monthly mean TGM concentration of 1.54 ng

276   m^{-3} in July was 0.43 ng m^{-3} higher than the lowest of 1.11 ng m^{-3} in November.

277   Measurements of TGM in other sites in the Tibetan Plateau also reported diverse seasonal patterns (Fig. 3). For example,

278   Fu et al. (2012a) found that at Waliguan the maximum TGM concentration was in January 2008, resulting from long-range

279   transport of pollutions from Northern India. Aside from January, monthly mean TGM concentrations at Waliguan had a clear

280   trend with high levels in warm seasons, and lower levels in cold seasons. The TGM variation at Mt. Gongga (Fu et al., 2008)

281   had a minimum in the summer, possibly due to the accelerated oxidation followed by dry deposition and wet scavenging

282   processes in the summer. The winter maximum of TGM at Mt. Gongga (Fu et al., 2008) implied the impact from anthropogenic

283   mercury emissions in the cold months. The seasonal variation of TGM at Shangri-La (Zhang et al., 2015) had high levels in

284   the spring and autumn, and low levels in the summer and winter which was different from all the other sites in the Tibetan

285   Plateau.

286   Compared to other high-altitude background sites in the mid-latitudes in Europe (Fig. 4) (Denzler et al., 2017; Fu et al.,

287   2016a; Ebinghaus et al., 2002) and sites in mid-latitudes in the US (Holmes et al., 2010; Weiss-Penzias et al., 2003; Sigler et

288   al., 2009; Yatavelli et al., 2006), the lower concentration of TGM at the Nam Co Station in the winter might be indicative of

289   atmospheric mercury removal in the winter caused by reactive halogens (Br and Br$_2$). The reaction rates for these reactions are

290   a strong inverse function of temperature (de Foy et al., 2016b; Goodsite et al., 2004), and they are accompanied by lower

surface ozone concentration (Yin et al., 2017), which is catalytically destroyed by halogens (Bottenheim et al., 1986; Obrist et al., 2011).

The summer peak of TGM at the Nam Co Station may be related to both the local re-emission of mercury from the earth's surface, and the long-range transport of mercury from South Asia (see details in section 3.5). At the Nam Co Station, daily mean TGM had a correlation coefficient with daily mean temperature reaching 0.56. Higher temperature in the warm seasons (Fig. 5) might lead to remobilization of soil mercury re-emission, which has been evidenced by a recent study on surface-air mercury exchange in the northern Tibetan Plateau (Ci et al., 2016). It is also possible that weaker wind speeds during the warm season (Fig. 5) suppressed the dilution of TGM with fresh air aloft in a low boundary layer. Furthermore, most precipitation happens in the summer at the Nam Co Station (You et al., 2007) and can increase emission of mercury from the Earth's surface by physical displacement of interstitial soil air by the infiltrating water (Ci et al., 2016) and by additional input of mercury from wet deposition (Huang et al., 2012). Besides local emissions, the summer monsoon can facilitate the transport of air masses with higher TGM concentrations from South Asia, and hence may also contribute to the summer peak of TGM.

The month of April in both 2012 and 2013 had higher monthly TGM levels than the months before and after (Fig. S3), possibly resulting from mercury emission from Nam Co Lake as the lake started to thaw in April (Gou et al., 2015).

3.3 Diurnal variations of TGM

Diurnal variations of TGM in different seasons exhibited a regular pattern, characterized by a sharp rise shortly after sunrise and a fairly steady decrease from the morning peak until sunset (Fig. 6). After sunset, TGM increased until midnight in the summer, the spring and the autumn. The diurnal variation of TGM at the Nam Co Station was similar to those of Mt. Gongga (Fu et al., 2009), Mt. Leigong (Fu et al., 2010), Mt. Changbai (Fu et al., 2012b), Mt. Waliguan (Fu et al., 2012a) and Reno (Peterson et al., 2009) except that the morning increase occurs earlier and is shorter compared during other sites that have a gradual increase throughout the morning.

Fig. 7 showed the comparison of TGM concentrations with a box model simulation by seasons. The best match in the box model was obtained by using variables including constant TGM reduction throughout the day, TGM increases at sunrise, TGM increases in the early evening, TGM dilution due to vertical mixing and a lifetime of TGM loss during daylight hours (Table 2). The R^2 of the model simulation ranged from 0.91 to 0.99, suggesting that the simulations reproduced the diurnal variations

accurately. As described above, both the measurements and the model have sharp bursts of TGM in the morning (7:00-9:00) and in the evening (18:00-22:00) during all seasons. Constant reductions existed in the spring, summer and autumn which would correspond to reduction rates of around 1 to 2 ng m^{-2} h^{-1}.

Fig. 8 showed the seasonal diurnal profiles of TGM and meteorological parameters. TGM concentrations were stable or slightly decreasing after midnight (0:00-6:00) under shallow nocturnal boundary layers. Notably, the morning increase of TGM happens immediately after sunrise, but before the increases of temperature, wind speed or humidity. The atmospheric mercury bursts in the morning (7:00-9:00) is probably due to prompt re-emission of nocturnal mercury deposition on the Earth's surface (Fu et al., 2016b; Howard et al., 2017; Kim 2010). The stable nocturnal boundary layer terminated at sunrise at which point mercury, including the mercury in the soil indigenously and/or deposited overnight, started to be reemitted into the shallow stable boundary layer before the increase of temperature which leads to an increase in the mixing height. As the temperature and radiation increased, so did the boundary layer height which developed into a convective mixed boundary layer and generated greater vertical mixing between the surface and loft. At the same time, the surface wind speed also increased. With increased vertical and horizontal dispersion, TGM released from the surface was diluted during the daytime (Liu et al., 2011; Lee et al., 1998). When the temperature decreased and the boundary layer converted back into a nocturnal boundary layer after sunset, depressed vertical mixing facilitated the build-up of TGM and such build-up was more significant in the warm seasons. In the evening, increases in TGM correspond to increases in specific humidity, especially in the summer.

3.4 Multiple linear regression and WRF-FLEXPART clusters results

Results of the MLR simulations for the entire measurement period (2012-2014) had a close correlation with the measurements: the correlation coefficient was 0.77 for all 12649 data points and 0.84 excluding the 383 outliers (Fig. 9). The primary contributor to the variance of the simulated time series was the seasonal signal, including the 12-month and 6-month harmonics as well as the smoothed specific humidity and temperature time series (Table 3). These were grouped together when presenting the results because they were not orthogonal to each other, and they contributed 84% of the variance of TGM in MLR simulation. The diurnal factors accounted for 4% of the variance, the WRF boundary layer heights accounted for 4% of the variance, and the local winds were associated with 1% of the variance. These factors showed that there was an impact from horizontal and vertical dispersion as well as daily cycling patterns due to either transport or chemistry, but that these factors

were considerably smaller than the seasonal variation at the site. Only 1% of the variance was associated with the annual signal, showing that the decrease in the concentrations reported in Sec. 3.1 was a small contributor to variations in TGM at Nam Co. The time series of surface ozone concentration contributed 3% to the variance and the stratospheric ozone tracer contributed 3%. We hypothesized that this was because ozone concentrations acted as an indicator of the oxidative potential of the air mass, although in the case of surface ozone concentration it could also be because they were a tracer of aged polluted air masses.

The regression analysis screens for high and low outliers. In particular, high outliers were significant in terms of TGM concentrations: they had an average concentration of 1.91 ng m^{-3} which is 0.58 ng m^{-3} higher than the average of the measurements retained in the simulations (Fig. 9). Fig. 9 showed that a number of the high outliers are associated with specific peak events, indicating that occasional plumes of high TGM are not associated with recurring emissions or periodically occurring conditions. A significant amount of TGM not accounted-for in the model was due to the high outliers. Additionally, a few events with very low TGM concentrations were not simulated. They have an average concentration of 0.9 ng m^{-3}. Fig. 10a showed the 6 wind transport clusters based on the hourly WRF-FLEXPART simulations. The figure showed the average residence time analysis for all the hours in each cluster, which characterizes the path of the air masses arriving at the measurement site for each cluster. The most frequent clusters were clusters 1 and 2 which accounted for 30% and 34% of measurement hours respectively. For measurement times during these clusters, the air masses clearly came from the west with a slight southern component for cluster 1 and a slight northern component in the case of cluster 2. Cluster 3 represented hours influenced by transport from the north which occurred during 15% of the measurement period. These were associated with the passage of storms at Nam Co: as the low pressure system moved to the east, the winds shifted from northwesterly to northeasterly. Clusters 4, 5 and 6 occurred less frequently and all represented different types of wind transport across the Himalayas from the south. Cluster 4 was the least frequent cluster, occurring 5% of the time. It included transport from the southeast including the northeastern corner of the Indo-Gangetic plain and occasional transport from southwestern China. This cluster also included transport from the direction of Lhasa. Cluster 5 occurred 7% of the time and represents transport from the south including Bangladesh. Cluster 6 occurred 9% of the time and included transport from Nepal and northern India.

The WRF-FLEXPART clusters were included in the MLR analysis and helped to improve the simulations for several tests. However, they did not increase the correlation coefficient of the final regression time series and consequently were not

included in the final MLR results. This could be because transport was already characterized by the other variables in the model such as temperature and humidity (which can serve as tracers of different air masses) and local wind speed and direction. Nevertheless, the importance of air mass transport can be seen from the probability density function of the TGM concentrations by cluster shown in Fig. 10b. Clusters 1 and 2, which had transport from the west, clearly had the lowest TGM concentrations. Next in terms of increasing TGM concentrations were clusters 3 and 6 which had transport from the north and from the southwest. TGM concentrations above 2 ng m^{-3} are very clearly associated with cluster 4 which has transport from the east and through Lhasa, which was also probably due to the further impact from eastern Indo-Gangetic Plain and the possibility of episodic transport events from China. Of the 87 hours with concentrations higher than 2 ng m^{-3}, 59% occurred during cluster 4 and 17% during cluster 5 with less than 8% for each of the other clusters. This demonstrated clearly that in addition to having the highest average levels, clusters 4 and 5 accounted for most of the peak concentrations.

3.5 HYSPLIT and PSCF results

Backward trajectories were calculated using HYSPLIT to identify the origins of air masses and associated TGM concentrations to the Nam Co Station. Most HYSPLIT trajectories originated from the west of Nam Co including the western and central Tibetan Plateau, the southwestern part of the Xinjiang Uygur Autonomous Region, South Asia, Central Asia and Western Asia. Very few trajectories originated from eastern China (Fig. S5). The backward trajectories were grouped into 6 clusters. Cluster 3 indicated the air mass from the south, originating from Bhutan and Bangladesh. This cluster had the lowest starting heights as well as traveling heights, but the highest mean TGM concentration (1.48 ng m^{-3}) (Table S2) in agreement with the FLEXPART results (Sec. 3.4). Clusters 1, 2, 4, 5 and 6 originated in the west, including air masses originating from northern India, Pakistan, Afghanistan and Iran passed over the Himalayas before arriving at the Nam Co Station. They had longer pathways through the Tibetan Plateau than Cluster 3. Cluster 4 had the longest transport route from the west, suggestive of faster wind speeds, and also the lowest TGM mean concentration (1.12 ng m^{-3}) with relatively high transport height.

PSCF calculations were based on concurrent TGM measurements and HYSPLIT backward trajectories, and thus can further constrain the potential source regions. Areas including IGP, the southern part of the Xinjiang Uygur Autonomous Region, the western part of Qinghai province and areas near the Nam Co Station in the Tibet Autonomous Region were identified as overall high potential sources regions and pathways (Fig. S6). Except for the areas near the Nam Co Station, these

391 potential sources regions correspond well with the atmospheric mercury emissions and biomass burning. The Bay of Bengal

392 was identified as a potential source region probably due to high emissions from its surroundings associated with frequent

393 occurrence of trajectories passing through this area in the summer.

394   Seasonal PSCFs were calculated in 2012 to investigate the potential sources by seasons (Fig. 11). In the spring, the autumn

395 and the winter, the Nam Co Station was dominated by the Westerlies. Pollutants from South Asia might be diluted by the clean

396 air during the transport within the Tibetan Plateau before they arrived at the Nam Co Station (Fig. S7). A zonal region in the

397 central IGP (Fig. 11) with elevated pollution represents a constant potential source (Gautam et al., 2011; Mallik and Lal, 2014).

398 The significant impact of long-range transport pollution from northwestern India on the Tibetan Plateau was also evidenced

399 by TGM measurements at Waliguan (Fu et al., 2012a). In the summer, the Indian Monsoon prevails and air masses arrived at

400 the Nam Co Station that had shorter pathway after entering the Tibetan Plateau than those in other seasons (Fig. S7). The

401 central IGP was again found to have higher PSCF values than other regions, even though these were much lower than the

402 PSCF values of other seasons. The highest PSCF values in the summer were in the eastern IGP (Fig. 11). For all seasons, the

403 region near the Nam Co Station, especially its south and west, was high in PSCF values all through the year, indicating that

404 air masses with high TGM concentrations predominantly came from the south-southwest.

405 **3.6 Implications for transboundary air pollution to the Tibetan Plateau**

406   The seasonal atmospheric circulation pattern in the Tibetan Plateau was characterized by the Indian monsoon in the

407 summer and the Westerlies in the winter. Such a climate regime exerted a profound impact on the seasonal atmospheric

408 environment by affecting the air transport dynamic and associated climate conditions. Pollutants like black carbon and

409 hexachlorocyclohexanes peaked in pre-monsoon season and declined during monsoon season at Nam Co and Lulang, resulting

410 from seasonal rainfall variations that can scavenge aerosols during their transport from source regions to the Tibetan Plateau

411 (Zhang et al., 2017; Wan et al., 2015; Sheng et al., 2013). In contrast, gaseous pollutants showed different seasonal patterns:

412 TGM at Nam Co in this study and persistent organic pollutants (dichlorodiphenyltrichloroethane and polychlorinated biphenyls)

413 at Lulang showed higher concentrations during the monsoon season compared to the pre-monsoon season (Sheng et al., 2013).

414 TGM at Nam Co showed strong covariance with temperature and specific humidity, all of which are in phase with the Indian

415 Monsoon Index (IMI) (Wang and Fan, 1999; Wang et al., 2001) (Fig. 12), indicating the importance of Indian Summer

Monsoon as a major driver delivering of transboundary transport of air pollution into the inland Tibetan Plateau. We suggested that gaseous pollutants were not readily deposited and/or washed out by precipitation during their transport and were more likely associated with the transport dynamics driven by the Indian Summer Monsoon, hence they showed high values when the Indian Summer Monsoon prevails. Transboundary air pollution was not the sole factor contributing to elevated TGM during summer: temperature-dependent processes such as gas-particle fractionation and surface reemission can also contribute to such seasonal patterns. Nonetheless, the close relationship between TGM and the Indian Summer Monsoon and the clear difference in seasonal patterns between gaseous and particulate pollutants together indicated that additional measurements of multiple pollutants and comparative studies are required to achieve a more comprehensive understanding and assessment of transboundary air pollution to the Tibetan Plateau.

4 Conclusions

We conducted three-years of TGM measurements at the Nam Co Station in the inland area of the Tibetan Plateau, China, from January 2012 to October 2014. The mean TGM concentration was 1.33 ± 0.24 ng m^{-3} during the whole measurement period and the low TGM level at the Nam Co Station indicated that the environment is pristine in the inland Tibetan Plateau. A weak decrease of TGM was identified over the course of the measurements.

In contrast to many other sites in China, TGM at the Nam Co Station showed high concentrations in warm seasons and low concentrations in cold seasons. Compared with other high-altitude background sites, the low concentration of TGM at the Nam Co Station in the winter may be due to the removal of mercury due to halogen. Seasonal variation of TGM at the Nam Co Station was influenced by factors such as re-emission processes of deposited mercury over the Earth's surfaces, vertical mixing and long-range transport. Multiple linear regression, backward trajectories and PSCF were investigated at the Nam Co Station and results indicated that long-range transports from the central and eastern Indo-Gangetic Plain were potentially the main sources for seasonally elevated TGM at the Nam Co Station due to the alternate impact of the Westerlies and of the Indian monsoon. Peak concentrations of TGM at the Nam Co Station were associated with air masses from the eastern Indo-Gangetic Plain with the possibility of episodic transport events from China.

At the Nam Co Station, the diurnal TGM profile had a peak 2-3 hours after sunrise and reached its lowest concentration before sunset. An exploratory box model simulation shows that this diurnal profile can be accurately represented using TGM

441 reductions 24 hours per day, TGM increases near sunrise and sunset, and dilution due to vertical mixing. Daily meteorology

442 conditions, such as high temperature, high solar radiation and more precipitation facilitated the Earth's surface mercury

443 emission. The decline of TGM concentrations in the daytime was likely due to vertical dilution from increased vertical mixing,

444 as well as due to the conversion of GEM to oxidized species that are easily deposited.

445   Due to the insolubility of TGM, which is different from particulate pollutant, TGM was less affected by the precipitation

446 during the transport in monsoon season and measurement of TGM at the Nam Co Station can continually reflect the

447 transboundary air pollution from the South Asia to the inland Tibetan Plateau.

448   The measurements of TGM at the Nam Co Station will be useful in providing atmospheric mercury baseline in the remote

449 inland Tibetan Plateau, improving the accuracy of modeled concentrations of TGM in the inland Tibetan Plateau, and serving

450 as new constraint for assessment of Asian mercury emission and pollution.

451

452   Data availability. All the data presented in this paper can be made available for scientific purposes upon request to the

453 corresponding authors (Qianggong Zhang (qianggong.zhang@itpcas.ac.cn) or Shichang Kang (shichang.kang@lzb.ac.cn)).

454

455 **Acknowledgements**

456   This study was supported by the National Natural Science Foundation of China (41630754 and 41630748) and Q. G.

457 Zhang acknowledges financial support from the Youth Innovation Promotion Association of CAS (2016070). X. F. Yin

458 acknowledges China Scholarship Council. The authors are grateful to Yaqiang Wang, who is the developer of MeteoInfo and

459 who provided generous help. The authors thank NOAA for providing the HYSPLIT model and GFS meteorological files.

460 Finally, the authors would like to thank the editor and referees of this paper for their helpful comments and suggestions.

461

462

463

464

465

References:

AMAP/UNEP: Technical Background Report for the Global Mercury Assessment 2013, Arctic Monitoring and Assessment Programme, 2013.

Ashbaugh, L. L., Malm, W. C., and Sadeh, W. Z.: A residence time probability analysis of sulfur concentrations at Grand Canyon National Park, Atmospheric Environment (1967), 19, 1263-1270, 1985.

Assessment, U. G. M.: Sources, Emissions, Releases and Environmental Transport, UNEP Chemicals Branch, Geneva, Switzerland, 42, 2013.

Bottenheim, J., Gallant, A. G., and Brice, K. A.: Measurements of NOy species and O_3 at 82 N latitude, Geophysical Research Letters, 13, 113-116, 1986.

Brioude, J., Arnold, D., Stohl, A., Cassiani, M., Morton, D., Seibert, P., Angevine, W., Evan, S., Dingwell, A., and Fast, J. D.: The Lagrangian particle dispersion model FLEXPART-WRF version 3.1, Geoscientific Model Development, 6, 1889-1904, 2013.

Burger Chakraborty, L., Qureshi, A., Vadenbo, C., and Hellweg, S.: Anthropogenic mercury flows in India and impacts of emission controls, Environmental science & technology, 47, 8105-8113, 2013.

Chen, L., Liu, M., Xu, Z., Fan, R., Tao, J., Chen, D., Zhang, D., Xie, D., and Sun, J.: Variation trends and influencing factors of total gaseous mercury in the Pearl River Delta—A highly industrialised region in South China influenced by seasonal monsoons, Atmospheric environment, 77, 757-766, 2013.

Choi, H.-D., and Holsen, T. M.: Gaseous mercury emissions from unsterilized and sterilized soils: the effect of temperature and UV radiation, Environmental Pollution, 157, 1673-1678, 2009.

Ci, Z., Peng, F., Xue, X., and Zhang, X.: Air–surface exchange of gaseous mercury over permafrost soil: an investigation at a high-altitude (4700 m asl) and remote site in the central Qinghai–Tibet Plateau, Atmospheric Chemistry and Physics, 16, 14741-14754, 2016.

Ci, Z., Zhang, X., Wang, Z., and Niu, Z.: Atmospheric gaseous elemental mercury (GEM) over a coastal/rural site downwind of East China: temporal variation and long-range transport, Atmospheric environment, 45, 2480-2487, 2011.

Cong, Z., Kang, S., Liu, X., and Wang, G.: Elemental composition of aerosol in the Nam Co region, Tibetan Plateau, during summer monsoon season, Atmospheric Environment, 41, 1180-1187, 2007.

Cong, Z., Kawamura, K., Kang, S., and Fu, P.: Penetration of biomass-burning emissions from South Asia through the Himalayas: new insights from atmospheric organic acids, Scientific reports, 5, 9580, 2015.

Davies, D., Kumar, S., and Descloitres, J.: Global Fire Monitoring Use of MODIS Near-real-time Satellite Data, GIM INTERNATIONAL, 18, 41-43, 2004.

Dou, H., Wang, S., Wang, L., Zhang, L., and Hao, J.: Characteristics of total gaseous mercury concentrations at a rural site of Yangtze Delta, China, Huan jing ke xue= Huanjing kexue, 34, 1-7, 2013.

de Foy, B., Wiedinmyer, C., and Schauer, J.: Estimation of mercury emissions from forest fires, lakes, regional and local sources using measurements in Milwaukee and an inverse method, Atmospheric Chemistry and Physics, 12, 8993-9011, 2012.

de Foy, B., Lu, Z., and Streets, D. G.: Impacts of control strategies, the great recession and weekday variations on NO_2 columns above North American cities, Atmospheric Environment, 138, 74-86, 2016a.

de Foy, B., Tong, Y., Yin, X., Zhang, W., Kang, S., Zhang, Q., Zhang, G., Wang, X., and Schauer, J. J.: First field-based atmospheric observation of the reduction of reactive mercury driven by sunlight, Atmospheric Environment, 134, 27-39, 2016b.

de Foy, B., Lu, Z., and Streets, D. G.: Satellite NO_2 retrievals suggest China has exceeded its NO_x reduction goals from the twelfth Five-Year Plan, Scientific reports, 6, 35912, 2016c.

de Foy, B.: City-level variations in NO x emissions derived from hourly monitoring data in Chicago, Atmospheric Environment, 2017.

Denzler, B., Bogdal, C., Henne, S., Obrist, D., Steinbacher, M., and Hungerbühler, K.: Inversion Approach to Validate Mercury Emissions Based on Background Air Monitoring at the High Altitude Research Station Jungfraujoch (3580 m), Environmental Science & Technology, 51, 2846-2853, 2017.

Draxler, R. R., and Rolph, G.: HYSPLIT (HYbrid Single-Particle Lagrangian Integrated Trajectory) model access via NOAA ARL READY website (http://www. arl. noaa. gov/ready/hysplit4. html). NOAA Air Resources Laboratory, Silver Spring, in, Md, 2003.

Ebinghaus, R., Kock, H., Coggins, A., Spain, T., Jennings, S., and, and Temme, C.: Long-term measurements of atmospheric mercury at Mace Head, Irish west coast, between 1995 and 2001, Atmospheric Environment, 36, 5267-5276, 2002.

Feng, X., Tang, S., Shang, L., Yan, H., Sommar, J., and Lindqvist, O.: Total gaseous mercury in the atmosphere of Guiyang, PR China, Science of the Total Environment, 304, 61-72, 2003.

Feng, X., Shang, L., Wang, S., Tang, S., and Zheng, W.: Temporal variation of total gaseous mercury in the air of Guiyang, China, Journal of Geophysical Research: Atmospheres, 109, 2004.

Fu, X., Feng, X., Zhu, W., Wang, S., and Lu, J.: Total gaseous mercury concentrations in ambient air in the eastern slope of Mt. Gongga, South-Eastern fringe of the Tibetan plateau, China, Atmospheric Environment, 42, 970-979, 2008.

Fu, X., Feng, X., Wang, S., Rothenberg, S., Shang, L., Li, Z., and Qiu, G.: Temporal and spatial distributions of total gaseous mercury concentrations in ambient air in a mountainous area in southwestern China: Implications for industrial and domestic mercury emissions in remote areas in China, Science of the total environment, 407, 2306-2314, 2009.

Fu, X., Feng, X., Dong, Z., Yin, R., Wang, J., Yang, Z., and Zhang, H.: Atmospheric gaseous elemental mercury (GEM) concentrations and mercury depositions at a high-altitude mountain peak in south China, Atmospheric Chemistry and Physics, 10, 2425-2437, 2010.

Fu, X., Feng, X., Qiu, G., Shang, L., and Zhang, H.: Speciated atmospheric mercury and its potential source in Guiyang, China, Atmospheric environment, 45, 4205-4212, 2011.

Fu, X., Feng, X., Liang, P., Zhang, H., Ji, J., and Liu, P.: Temporal trend and sources of speciated atmospheric mercury at Waliguan GAW station, Northwestern China, Atmospheric Chemistry and Physics, 12, 1951-1964, 2012a.

Fu, X., Feng, X., Shang, L., Wang, S., and Zhang, H.: Two years of measurements of atmospheric total gaseous mercury (TGM) at a remote site in Mt. Changbai area, Northeastern China, Atmospheric Chemistry and Physics, 12, 4215-4226, 2012b.

Fu, X., Feng, X., Sommar, J., and Wang, S.: A review of studies on atmospheric mercury in China, Science of the Total Environment, 421, 73-81, 2012c.

Fu, X., Marusczak, N., Heimbürger, L.-E., Sauvage, B., Gheusi, F., Prestbo, E. M., and Sonke, J. E.: Atmospheric mercury speciation dynamics at the high-altitude Pic du Midi Observatory, southern France, Atmos. Chem. Phys, 16, 5623-5639, 2016a.

Fu, X., Zhang, H., Yu, B., Wang, X., Lin, C.-J., and Feng, X.: Observations of atmospheric mercury in China: a critical review, Atmos. Chem. Phys, 15, 9455-9476, 2015.

Fu, X., Zhu, W., Zhang, H., Sommar, J., Yu, B., Yang, X., Wang, X., Lin, C.-J., and Feng, X.: Depletion of atmospheric gaseous elemental mercury by plant uptake at Mt. Changbai, Northeast China, Atmospheric Chemistry and Physics, 16, 12861-12873, 2016b.

Gautam, R., Hsu, N., Tsay, S., Lau, K., Holben, B., Bell, S., Smirnov, A., Li, C., Hansell, R., and Ji, Q.: Accumulation of aerosols over the Indo-Gangetic plains and southern slopes of the Himalayas: distribution, properties and radiative effects during the 2009 pre-monsoon season, Atmospheric Chemistry and Physics, 11, 12841-12863, 2011.

Giglio, L., Descloitres, J., Justice, C. O., and Kaufman, Y. J.: An enhanced contextual fire detection algorithm for MODIS, Remote sensing of environment, 87, 273-282, 2003.

Goodsite, M. E., Plane, J., and Skov, H.: A theoretical study of the oxidation of Hg^0 to $HgBr_2$ in the troposphere, Environmental science & technology, 38, 1772-1776, 2004.

Gratz, L., Esposito, G., Dalla Torre, S., Cofone, F., Pirrone, N., and Sprovieri, F.: First Measurements of Ambient Total Gaseous Mercury (TGM) at the EvK2CNR Pyramid Observatory in Nepal, E3S Web of Conferences, 2013.

Holmes, C. D., Jacob, D. J., Corbitt, E. S., Mao, J., Yang, X., Talbot, R., and Slemr, F.: Global atmospheric model for mercury including oxidation by bromine atoms, Atmospheric Chemistry and Physics, 10, 12037-12057, 2010.

Horowitz, H. M., Jacob, D. J., Zhang, Y., Dibble, T. S., Slemr, F., Amos, H. M., Schmidt, J. A., Corbitt, E. S., Marais, E. A., and Sunderland, E. M.: A new mechanism for atmospheric mercury redox chemistry: implications for the global mercury budget, Atmospheric Chemistry and Physics, 17, 6353-6371, 2017.

Howard, D., and Edwards, G. C.: Mercury fluxes over an Australian alpine grassland and observation of nocturnal atmospheric mercury depletion events, Atmos. Chem. Phys. Discuss., https://doi. org/10.5194/acp-2017-580, in review, 2017.

Huang, J., Kang, S., Zhang, Q., Yan, H., Guo, J., Jenkins, M. G., Zhang, G., and Wang, K.: Wet deposition of mercury at a remote site in the Tibetan Plateau: concentrations, speciation, and fluxes, Atmospheric Environment, 62, 540-550, 2012.

Huang, J., Kang, S., Wang, S., Wang, L., Zhang, Q., Guo, J., Wang, K., Zhang, G., and Tripathee, L.: Wet deposition of mercury at Lhasa, the capital city of Tibet, Science of the total environment, 447, 123-132, 2013.

Huang, J., Kang, S., Guo, J., Zhang, Q., Cong, Z., Sillanpää, M., Zhang, G., Sun, S., and Tripathee, L.: Atmospheric particulate mercury in Lhasa city, Tibetan Plateau, Atmospheric Environment, 142, 433-441, 2016.

Kang, S., Huang, J., Wang, F., Zhang, Q., Zhang, Y., Li, C., Wang, L., Chen, P., Sharma, C. M., and Li, Q.: Atmospheric mercury depositional chronology reconstructed from lake sediments and ice core in the Himalayas and Tibetan Plateau, Environmental science & technology, 50, 2859-2869, 2016.

Karunasagar, D., Krishna, M. B., Anjaneyulu, Y. a., and Arunachalam, J.: Studies of mercury pollution in a lake due to a thermometer factory situated in a tourist resort: Kodaikkanal, India, Environmental pollution, 143, 153-158, 2006.

Kellerhals, M., Beauchamp, S., Belzer, W., Blanchard, P., Froude, F., Harvey, B., McDonald, K., Pilote, M., Poissant,

L., and Puckett, K.: Temporal and spatial variability of total gaseous mercury in Canada: results from the Canadian Atmospheric Mercury Measurement Network (CAMNet), Atmospheric Environment, 37, 1003-1011, 2003.

Kim, S. Y.: Continental outflow of polluted air from the US to the North Atlantic and mercury chemical cycling in various atmospheric environments, University of New Hampshire (Natural Resources and Earth Systems Science Program), 2010.

Kock, H., Bieber, E., Ebinghaus, R., Spain, T., and Thees, B.: Comparison of long-term trends and seasonal variations of atmospheric mercury concentrations at the two European coastal monitoring stations Mace Head, Ireland, and Zingst, Germany, Atmospheric Environment, 39, 7549-7556, 2005.

Kocman, D., and Horvat, M.: A laboratory based experimental study of mercury emission from contaminated soils in the River Idrijca catchment, Atmospheric Chemistry and Physics, 10, 1417-1426, 2010.

Lan, X., Talbot, R., Castro, M., Perry, K., and Luke, W.: Seasonal and diurnal variations of atmospheric mercury across the US determined from AMNet monitoring data, Atmospheric Chemistry and Physics, 12, 10569, 2012.

Landis, M. S., Stevens, R. K., Schaedlich, F., and Prestbo, E. M.: Development and characterization of an annular denuder methodology for the measurement of divalent inorganic reactive gaseous mercury in ambient air, Environmental science & technology, 36, 3000-3009, 2002.

Larsen, L., Thomas, C., Eppinga, M., and Coulthard, T.: Exploratory modeling: Extracting causality from complexity, Eos, Transactions American Geophysical Union, 95, 285-286, 2014.

Li, C., Kang, S., Zhang, Q., and Kaspari, S.: Major ionic composition of precipitation in the Nam Co region, Central Tibetan Plateau, Atmospheric Research, 85, 351-360, 2007.

Li, C., Bosch, C., Kang, S., Andersson, A., Chen, P., Zhang, Q., Cong, Z., Chen, B., Qin, D., and Gustafsson, Ö.: Sources of black carbon to the Himalayan–Tibetan Plateau glaciers, Nature Communications, 7, 12574, 2016.

Li, Z., Xia, C., Wang, X., Xiang, Y., and Xie, Z.: Total gaseous mercury in Pearl River Delta region, China during 2008 winter period, Atmospheric Environment, 45, 834-838, 2011.

Lin, C.-J., and Pehkonen, S. O.: The chemistry of atmospheric mercury: a review, Atmospheric Environment, 33, 2067-2079, 1999.

Lindberg, S. a., and Stratton, W.: Atmospheric mercury speciation: concentrations and behavior of reactive gaseous mercury in ambient air, Environmental Science & Technology, 32, 49-57, 1998.

Liu, M., Chen, L., Xie, D., Sun, J., He, Q., Cai, L., Gao, Z., and Zhang, Y.: Monsoon-driven transport of atmospheric mercury to the South China Sea from the Chinese mainland and Southeast Asia—Observation of gaseous elemental mercury at a background station in South China, Environmental Science and Pollution Research, 23, 21631-21640, 2016.

Liu, N., Qiu, G., Landis, M. S., Feng, X., Fu, X., and Shang, L.: Atmospheric mercury species measured in Guiyang, Guizhou province, southwest China, Atmospheric Research, 100, 93-102, 2011.

Liu, Y., Wang, Y., Pan, Y., and Piao, S.: Wet deposition of atmospheric inorganic nitrogen at five remote sites in the Tibetan Plateau, Atmospheric Chemistry and Physics, 15, 11683-11700, 2015.

Ma, Y., Kang, S., Zhu, L., Xu, B., Tian, L., and Yao, T.: ROOF OF THE WORLD: Tibetan observation and research platform: atmosphere–land interaction over a heterogeneous landscape, Bulletin of the American Meteorological Society, 89, 1487-1492, 2008.

Mallik, C., and Lal, S.: Seasonal characteristics of SO2, NO2, and CO emissions in and around the Indo-Gangetic Plain, Environmental monitoring and assessment, 186, 1295-1310, 2014.

Mukherjee, A. B., Bhattacharya, P., Sarkar, A., and Zevenhoven, R.: Mercury emissions from industrial sources in India and its effects in the environment, in: Mercury Fate and Transport in the Global Atmosphere, Springer, 81-112, 2009.

Müller, D., Wip, D., Warneke, T., Holmes, C., Dastoor, A., and Notholt, J.: Sources of atmospheric mercury in the tropics: continuous observations at a coastal site in Suriname, Atmospheric Chemistry and Physics, 12, 7391-7397, 2012.

Obrist, D., Tas, E., Peleg, M., Matveev, V., Faïn, X., Asaf, D., and Luria, M.: Bromine-induced oxidation of mercury in the mid-latitude atmosphere, Nature Geoscience, 4, 22-26, 2011.

Pacyna, E. G., Pacyna, J., Sundseth, K., Munthe, J., Kindbom, K., Wilson, S., Steenhuisen, F., and Maxson, P.: Global emission of mercury to the atmosphere from anthropogenic sources in 2005 and projections to 2020, Atmospheric Environment, 44, 2487-2499, 2010.

Park, S.-Y., Holsen, T. M., Kim, P.-R., and Han, Y.-J.: Laboratory investigation of factors affecting mercury emissions from soils, Environmental earth sciences, 72, 2711-2721, 2014.

Parvathi, K., Jayaprakash, K., and Sivakumar, N.: Mercury contamination due to thermometer glass solid waste dumping-a preliminary report, Asian Journal of Experimental Chemistry, 5, 46-48, 2010.

Peng, G., Qinghua, Y., and Qiufang, W.: Lake ice change at the Nam Co Lake on the Tibetan Plateau during 2000-2013 and influencing factors, PROGRESS IN GEOGRAPHY, 34, 1241-1249.

Peterson, C., Gustin, M., and Lyman, S.: Atmospheric mercury concentrations and speciation measured from 2004 to 2007 in Reno, Nevada, USA, Atmospheric Environment, 43, 4646-4654, 2009.

Pirrone, N., Cinnirella, S., Feng, X., Finkelman, R., Friedli, H., Leaner, J., Mason, R., Mukherjee, A., Stracher, G., and Streets, D.: Global mercury emissions to the atmosphere from anthropogenic and natural sources, Atmospheric Chemistry and Physics, 10, 5951-5964, 2010.

Poissant, L., Pilote, M., Beauvais, C., Constant, P., and Zhang, H. H.: A year of continuous measurements of three atmospheric mercury species (GEM, RGM and Hg p) in southern Quebec, Canada, Atmospheric Environment, 39, 1275-1287, 2005.

Polissar, A., Hopke, P., Paatero, P., Kaufmann, Y., Hall, D., Bodhaine, B., Dutton, E., and Harris, J.: The aerosol at Barrow, Alaska: long-term trends and source locations, Atmospheric Environment, 33, 2441-2458, 1999.

Rao, S., Zurbenko, I., Neagu, R., Porter, P., Ku, J., and Henry, R.: Space and time scales in ambient ozone data, Bulletin of the American Meteorological Society, 78, 2153-2166, 1997.

Schroeder, W. H., and Munthe, J.: Atmospheric mercury—an overview, Atmospheric Environment, 32, 809-822, 1998.

Selin, H.: Global environmental law and treaty-making on hazardous substances: the Minamata Convention and mercury abatement, Global Environmental Politics, 14, 1-19, 2014.

Sheng, J., Wang, X., Gong, P., Joswiak, D. R., Tian, L., Yao, T., and Jones, K. C.: Monsoon-driven transport of organochlorine pesticides and polychlorinated biphenyls to the Tibetan Plateau: three year atmospheric monitoring study, Environmental science & technology, 47, 3199-3208, 2013.

Shia, R. L., Seigneur, C., Pai, P., Ko, M., and Sze, N. D.: Global simulation of atmospheric mercury concentrations and deposition fluxes, Journal of Geophysical Research: Atmospheres, 104, 23747-23760, 1999.

Shichang, K., Yongping, Y., and Liping, Z.: Modern Environmental Process and Changes in the Basin of Nam Co in Tibetan Plateau, in, Beijing: China Meteorological Press (in Chinese with English abstract), 2011.

Sigler, J., Mao, H., and Talbot, R.: Gaseous elemental and reactive mercury in Southern New Hampshire, Atmospheric Chemistry and Physics, 9, 1929-1942, 2009.

Slemr, F., Brunke, E.-G., Ebinghaus, R., and Kuss, J.: Worldwide trend of atmospheric mercury since 1995, Atmospheric Chemistry and Physics, 11, 4779-4787, 2011.

Slemr, F., Brunke, E. G., Labuschagne, C., and Ebinghaus, R.: Total gaseous mercury concentrations at the Cape Point GAW station and their seasonality, Geophysical Research Letters, 35, 2008.

Sprovieri, F., Pirrone, N., Bencardino, M., D'Amore, F., Carbone, F., Cinnirella, S., Mannarino, V., Landis, M., Ebinghaus, R., and Weigelt, A.: Atmospheric mercury concentrations observed at ground-based monitoring sites globally distributed in the framework of the GMOS network, Atmospheric Chemistry and Physics, 16, 11915-11935, 2016.

Streets, D. G., Hao, J., Wu, Y., Jiang, J., Chan, M., Tian, H., and Feng, X.: Anthropogenic mercury emissions in China, Atmospheric Environment, 39, 7789-7806, 2005.

Su, J., Cheng, J.-p., Ye, X., Yuan, T., Wang, W., and Mi, L.: Preliminary study on mercury distribution in multimedia environment in Lanzhou, Journal of Agro-Environment Science, 26, 381-385, 2007.

Subramanian, V.: Water quality in south Asia, Asian journal of water, Environment and Pollution, 1, 41-54, 2004.

Sun, X., Wang, K., Kang, S., Guo, J., Zhang, G., Huang, J., Cong, Z., Sun, S., and Zhang, Q.: The role of melting alpine glaciers in mercury export and transport: An intensive sampling campaign in the Qugaqie Basin, inland Tibetan Plateau, Environmental pollution, 220, 936-945, 2017.

Sun, X., Zhang, Q., Kang, S., Guo, J., Li, X., Yu, Z., Zhang, G., Qu, D., Huang, J., and Cong, Z.: Mercury speciation and distribution in a glacierized mountain environment and their relevance to environmental risks in the inland Tibetan Plateau, Science of The Total Environment, 631, 270-278, 2018.

Tong, Y., Yin, X., Lin, H., Wang, H., Deng, C., Chen, L., Li, J., Zhang, W., Schauer, J. J., and Kang, S.: Recent Decline of Atmospheric Mercury Recorded by Androsace tapete on the Tibetan Plateau, Environmental Science & Technology, 50, 13224-13231, 2016.

Wan, Q., Feng, X., Lu, J., Zheng, W., Song, X., Han, S., and Xu, H.: Atmospheric mercury in Changbai Mountain area, northeastern China I. The seasonal distribution pattern of total gaseous mercury and its potential sources, Environmental research, 109, 201-206, 2009.

Wan, X., Kang, S., Wang, Y., Xin, J., Liu, B., Guo, Y., Wen, T., Zhang, G., and Cong, Z.: Size distribution of carbonaceous aerosols at a high-altitude site on the central Tibetan Plateau (Nam Co Station, 4730 m asl), Atmospheric Research, 153, 155-164, 2015.

Wang, B., and Fan, Z.: Choice of South Asian summer monsoon indices, Bulletin of the American Meteorological Society, 80, 629-638, 1999.

Wang, B., Wu, R., and Lau, K.: Interannual variability of the Asian summer monsoon: Contrasts between the Indian and the western North Pacific–East Asian monsoons, Journal of climate, 14, 4073-4090, 2001.

Wang, Y., Zhang, X., and Draxler, R. R.: TrajStat: GIS-based software that uses various trajectory statistical analysis methods to identify potential sources from long-term air pollution measurement data, Environmental Modelling & Software,

24, 938-939, 2009.

Wang, Y.: MeteoInfo: GIS software for meteorological data visualization and analysis, Meteorological Applications, 21, 360-368, 2014.

Wang, Y., Zhang, Y., Schauer, J. J., de Foy, B., Guo, B., and Zhang, Y.: Relative impact of emissions controls and meteorology on air pollution mitigation associated with the Asia-Pacific Economic Cooperation (APEC) conference in Beijing, China, Science of The Total Environment, 571, 1467-1476, 2016.

Wang, Y., de Foy, B., Schauer, J. J., Olson, M. R., Zhang, Y., Li, Z., and Zhang, Y.: Impacts of regional transport on black carbon in Huairou, Beijing, China, Environmental Pollution, 221, 75-84, 2017.

Weiss-Penzias, P., Jaffe, D. A., McClintick, A., Prestbo, E. M., and Landis, M. S.: Gaseous elemental mercury in the marine boundary layer: Evidence for rapid removal in anthropogenic pollution, Environmental science & technology, 37, 3755-3763, 2003.

Wu, Q., Wang, S., Li, G., Liang, S., Lin, C.-J., Wang, Y., Cai, S., Liu, K., and Hao, J.: Temporal Trend and Spatial Distribution of Speciated Atmospheric Mercury Emissions in China During 1978–2014, Environmental Science & Technology, 50, 13428-13435, 2016.

Wu, Q., Gao, W., Wang, S., and Hao, J.: Updated atmospheric speciated mercury emissions from iron and steel production in China during 2000–2015, Atmospheric Chemistry and Physics, 17, 10423-10433, 2017.

Xia, X., Zong, X., Cong, Z., Chen, H., Kang, S., and Wang, P.: Baseline continental aerosol over the central Tibetan plateau and a case study of aerosol transport from South Asia, Atmospheric environment, 45, 7370-7378, 2011.

Xiao, H., Shen, L., Su, Y., Barresi, E., DeJong, M., Hung, H., Lei, Y.-D., Wania, F., Reiner, E. J., and Sverko, E.: Atmospheric concentrations of halogenated flame retardants at two remote locations: The Canadian High Arctic and the Tibetan Plateau, Environmental pollution, 161, 154-161, 2012.

Xiu, G., Cai, J., Zhang, W., Zhang, D., Büeler, A., Lee, S., Shen, Y., Xu, L., Huang, X., and Zhang, P.: Speciated mercury in size-fractioned particles in Shanghai ambient air, Atmospheric Environment, 43, 3145-3154, 2009.

Xu, L., Chen, J., Yang, L., Niu, Z., Tong, L., Yin, L., and Chen, Y.: Characteristics and sources of atmospheric mercury speciation in a coastal city, Xiamen, China, Chemosphere, 119, 530-539, 2015.

Yang, H., Battarbee, R. W., Turner, S. D., Rose, N. L., Derwent, R. G., Wu, G., and Yang, R.: Historical reconstruction of mercury pollution across the Tibetan Plateau using lake sediments, Environmental science & technology, 44, 2918-2924, 2010.

Yaqiong, L., Yaoming, M., and Maoshan, L.: Study on characteristic of atmospheric boundary layer over Lake Namco region, Tibetan Plateau, Plateau Meteorology (in Chinese), 27, 1205-1210, 2008.

Yatavelli, R. L., Fahrni, J. K., Kim, M., Crist, K. C., Vickers, C. D., Winter, S. E., and Connell, D. P.: Mercury, PM 2.5 and gaseous co-pollutants in the Ohio River Valley region: Preliminary results from the Athens supersite, Atmospheric environment, 40, 6650-6665, 2006.

Yin, X., Kang, S., de Foy, B., Cong, Z., Luo, J., Lang, Z., Ma, Y., Zhang, G., Rupakheti, D., and Zhang, Q.: Surface ozone at Nam Co in the inland Tibetan Plateau: variation, synthesis comparison and regional representativeness, Atmospheric Chemistry and Physics, 17, 11293-11311, 2017.

You, Q., Kang, S., Li, C., Li, M., and Liu, J.: Variation features of meteorological elements at Namco Station, Tibetan

725 Plateau, Meteorological Monthly, 33, 54-60, 2007.

726   Yu, B., Wang, X., Lin, C. J., Fu, X., Zhang, H., Shang, L., and Feng, X.: Characteristics and potential sources of
727 atmospheric mercury at a subtropical near‐coastal site in East China, Journal of Geophysical Research: Atmospheres, 120,
728 8563-8574, 2015.

729   Zhang, L., Wang, S., Wang, L., and Hao, J.: Atmospheric mercury concentration and chemical speciation at a rural site
730 in Beijing, China: implications of mercury emission sources, Atmospheric Chemistry and Physics, 13, 10505-10516, 2013.

731   Zhang, Q., Pan, K., Kang, S., Zhu, A., and Wang, W.-X.: Mercury in wild fish from high-altitude aquatic ecosystems in
732 the Tibetan Plateau, Environmental science & technology, 48, 5220-5228, 2014.

733   Zhang, H., Fu, X., Lin, C., Wang, X., and Feng, X.: Observation and analysis of speciated atmospheric mercury in
734 Shangri-La, Tibetan Plateau, China, Atmos. Chem. Phys, 15, 653-665, 2015.

735   Zhang, X., Ming, J., Li, Z., Wang, F., and Zhang, G.: The online measured black carbon aerosol and source orientations
736 in the Nam Co region, Tibet, Environmental Science and Pollution Research, 24, 25021-25033, 2017.

737   Zhang, Y., Jacob, D. J., Horowitz, H. M., Chen, L., Amos, H. M., Krabbenhoft, D. P., Slemr, F., Louis, V. L. S., and
738 Sunderland, E. M.: Observed decrease in atmospheric mercury explained by global decline in anthropogenic emissions,
739 Proceedings of the National Academy of Sciences, 113, 526-531, 2016.

740   Zhu, J., Wang, T., Talbot, R., Mao, H., Hall, C., Yang, X., Fu, C., Zhuang, B., Li, S., and Han, Y.: Characteristics of
741 atmospheric total gaseous mercury (TGM) observed in urban Nanjing, China, Atmospheric Chemistry and Physics, 12,
742 12103-12118, 2012.

743
744
745
746
747
748
749
750
751
752
753
754
755
756
757
758
759
760
761

762

763 **Table 1. The statistics of TGM and meteorological variables in different seasons at the Nam Co Station during the measurement**

764 **period (2012-2014).**

Period	Statistical	TGM (ng m^{-3})	T (℃)	RH (%)	WS (m s^{-1})
Total	Mean	1.33	-0.29	50.67	3.32
	Median	1.34	0.30	50.00	2.80
	Standard Deviation	0.24	8.98	22.37	2.22
	Minimum	0.23	-28.90	5.30	0.00
	Maximum	3.14	19.00	98.00	15.60
	Count	14408	20695	20695	20695
Spring (MAM)	Mean	1.28	-0.90	51.58	3.21
	Median	1.30	-0.60	50.30	2.80
	Standard Deviation	0.20	6.48	24.38	2.11
	Minimum	0.42	-21.20	5.30	0.00
	Maximum	2.41	17.90	98.00	12.80
	Count	4506	4980	4980	4980
Summer (JJA)	Mean	1.50	8.80	63.32	2.94
	Median	1.50	8.60	65.30	2.60
	Standard Deviation	0.20	3.59	18.25	1.74
	Minimum	0.23	-4.10	11.00	0.00
	Maximum	3.14	19.00	97.00	11.10
	Count	5243	5805	5805	5805
Autumn (SON)	Mean	1.22	-0.78	47.06	3.36
	Median	1.20	-0.40	46.00	2.90
	Standard Deviation	0.17	7.23	20.55	2.07
	Minimum	0.87	-24.80	8.00	0.00
	Maximum	2.68	14.60	97.00	12.90
	Count	2267	4800	4800	4800
Winter (DJF)	Mean	1.14	-9.57	38.81	3.83
	Median	1.13	-9.00	36.00	3.00
	Standard Deviation	0.18	6.40	18.36	2.78
	Minimum	0.45	-28.90	7.00	0.00
	Maximum	2.08	5.20	91.70	15.60
	Count	2392	5110	5110	5110

765
766
767

Table 2. Statistics of free parameters in the box model of TGM at the Nam Co Station by seasons.

	Initial TGM (ng m⁻³)	Morning TGM (7-9) burst (ng m⁻²h⁻¹)	Evening TGM (18-22) burst (ng m⁻²h⁻¹)	Constant TGM deposition (ng m⁻²h⁻¹)	Free tropospheric TGM (ng m⁻³)	TGM lifetime during daylight (day)	root-mean-square error (RMSE)	R^2
Spring	1.288	58.29	37.66	-1.658	1.228	3.183	0.00983	0.96
Summer	1.521	14.2	25.65	-1.775	1.553	5.991	0.00796	0.91
Autumn	1.211	53.34	9.144	-1.061	1.036	Inf	0.0086	0.93
Winter	1.115	52.92	2.468	0	1.168	2.984	0.00368	0.99

	Initial TGM (ng m⁻³)	Morning TGM (7-9) burst (ng m⁻²h⁻¹)	Evening TGM (18-22) burst (ng m⁻²h⁻¹)	Constant TGM deposition (ng m⁻²h⁻¹)	Free tropospheric TGM (ng m⁻³)	TGM lifetime during daylight (day)	root-mean-square error (RMSE)	R^2

Table 3. Contribution from the different groups to the total variance of the model. The standard deviation of each group gives a sense of the contribution of each group to the variance in units of ng m^{-3}. The variance contribution shows the percentage that each group contributes to the total variance of the model.

Group name	No. Variables	Std (ng m^{-3})	Variance Contribution (%)
Seasonal Signal	6	0.161	83.70
Diurnal Signal	24	0.036	4.08
WRF PBLH	5	0.034	3.81
Surface O$_3$ Conc	1	0.032	3.20
Strat. O$_3$ Tracer	1	0.031	3.04
Local Winds	20	0.020	1.34
Annual Signal	43	0.016	0.86

822

823
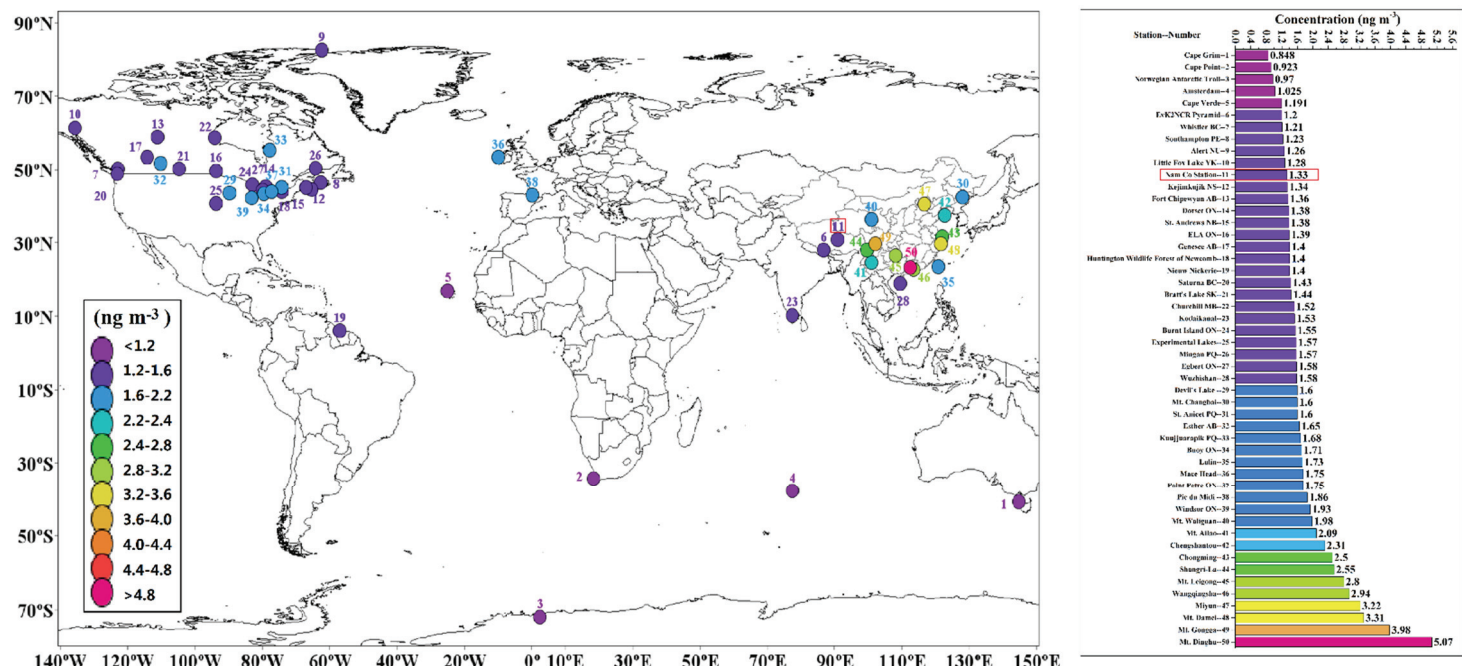
824   **Fig. 1. Geographical location of the remote and rural sites with atmospheric mercury measurements.**

825

826

827

828

829

830

831

832

833

834

835

836

837

838

839

840

841
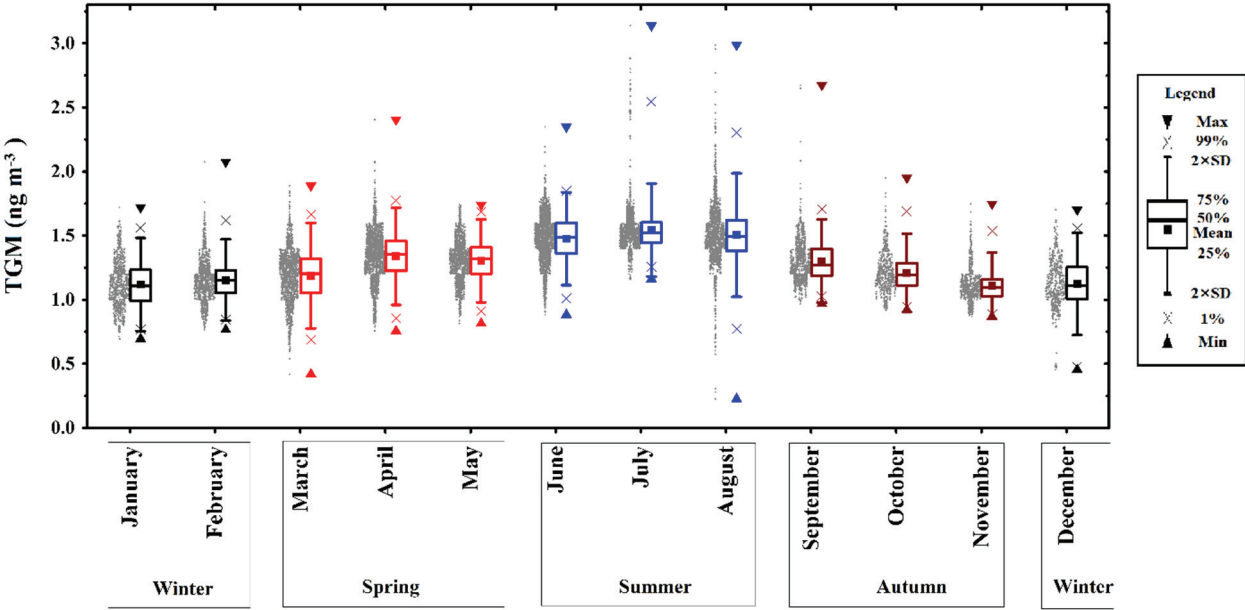
Fig. 2. Monthly average and statistical parameters of TGM at the Nam Co Station during the whole measurement period (spring (MAM) in red; summer (JJA) in blue; autumn (SON) in dark red; winter (DJF) in black).

843
844
845
846
847
848
849
850
851
852
853
854
855
856
857
858
859
860
861
862

863
864
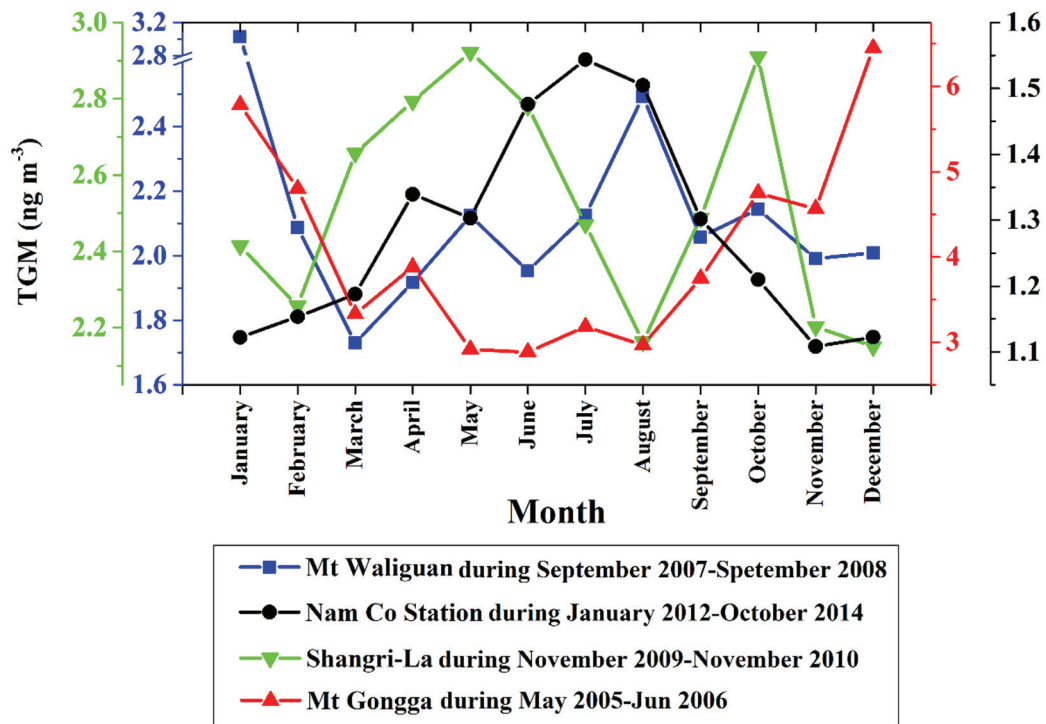
865
866
867 **Fig. 3. Variations of monthly mean TGM at four sites (Mt. Waliguan (Fu et al., 2012a), Nam Co, Mt. Gongga (Fu et al., 2008) and**
868 **Shangri-La (Zhang et al., 2015)) in the Tibetan Plateau.**
869
870
871
872
873
874
875
876
877
878
879
880
881
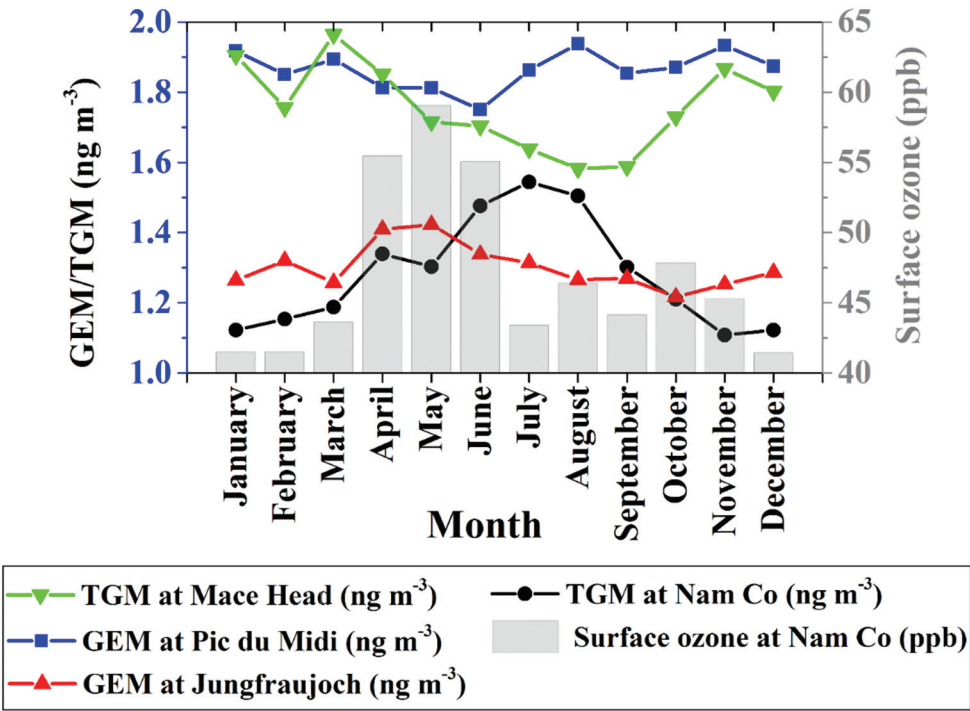
Fig. 4. Monthly average GEM/TGM at the Nam Co Station and three high-altitude background stations in the Northern

Hemisphere (Denzler et al., 2017; Fu et al., 2016a; Ebinghaus et al., 2002) (average TGM at Mace Head in green; average GEM at

Pic du Midi in blue; median GEM at Jungfraujoch in red; average TGM at the Nam Co Station in black); and monthly average

surface ozone at Nam Co in column.

902
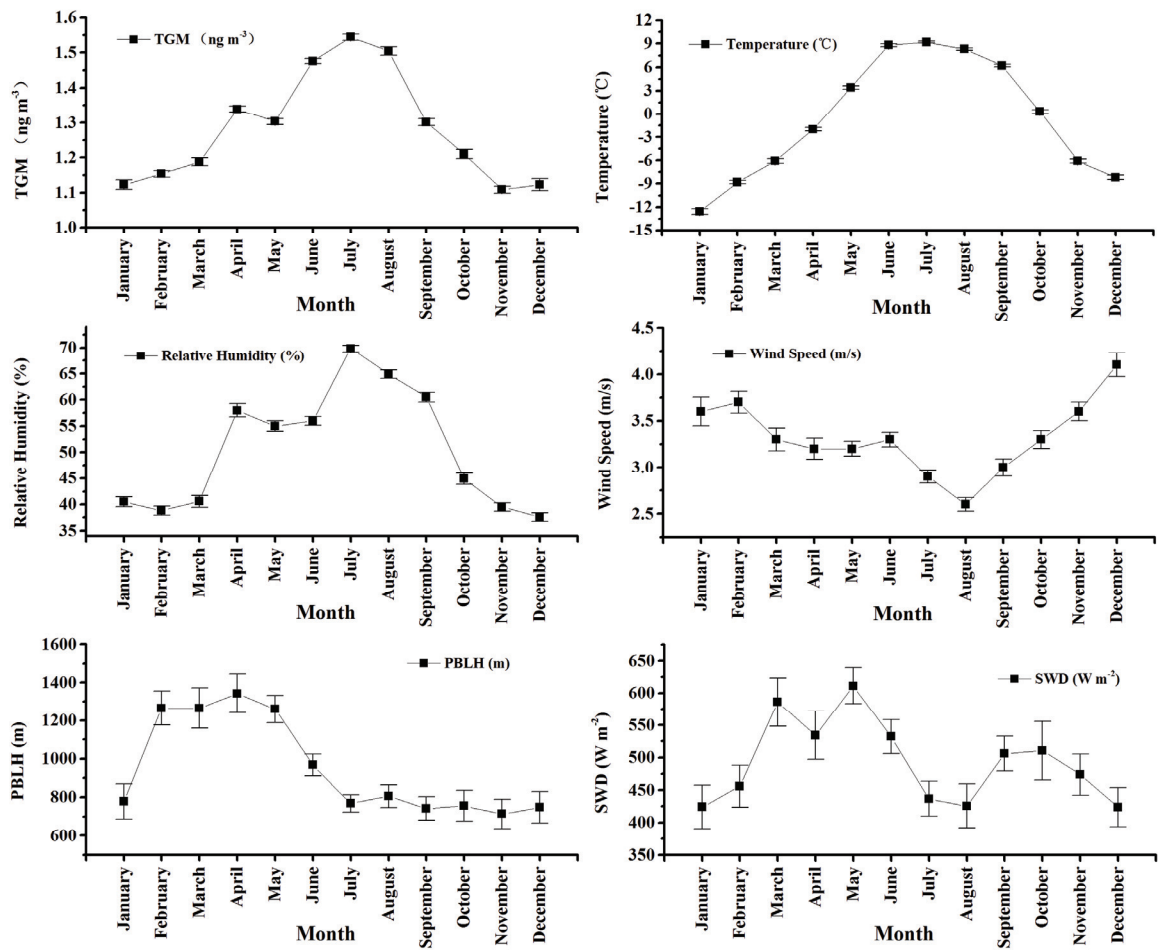
Fig. 5. Monthly variations of TGM, relative humidity, temperature, SWD (downward shortwave radiation), wind speed and PBLH (planetary boundary layer height) during the whole measurement period at the Nam Co Station. Error bars are 95% confidence levels.

903
904
905
906
907
908
909
910
911
912
913
914
915
916

917
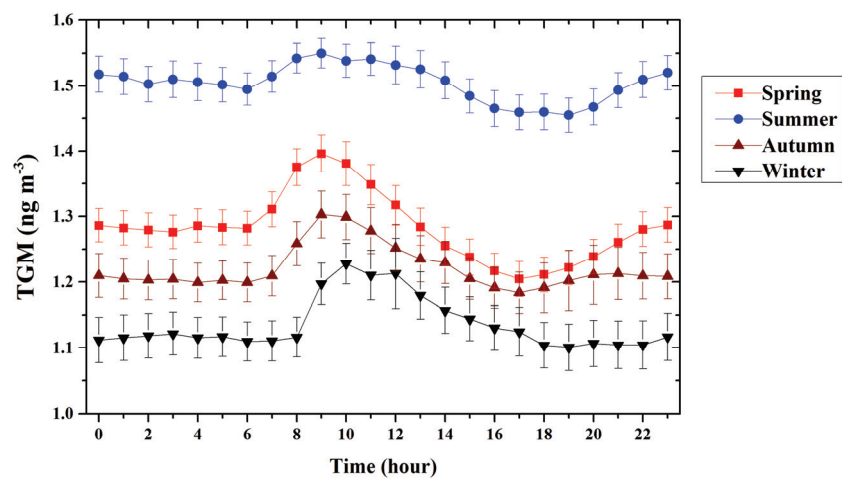
Fig. 6. Diurnal profiles of average hourly TGM at the Nam Co Station by seasons during the measurement period. Error bars are

95% confidence levels.

918
919
920
921
922
923
924
925
926
927
928
929
930
931
932
933
934
935
936
937
938
939
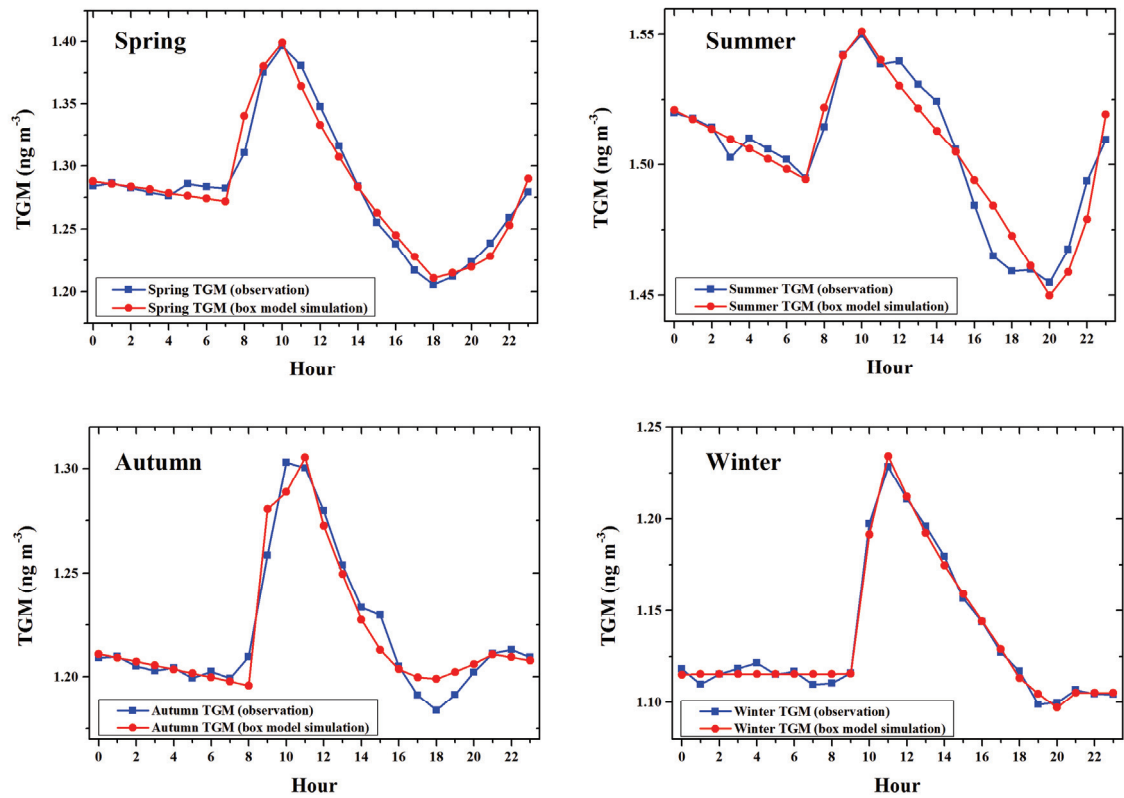
942   **Fig. 7. Diurnal profiles of average hourly TGM at the Nam Co Station by seasons during the measurement period compared with**
943   **box model simulation.**

944
945
946
947
948
949
950
951
952
953
954
955
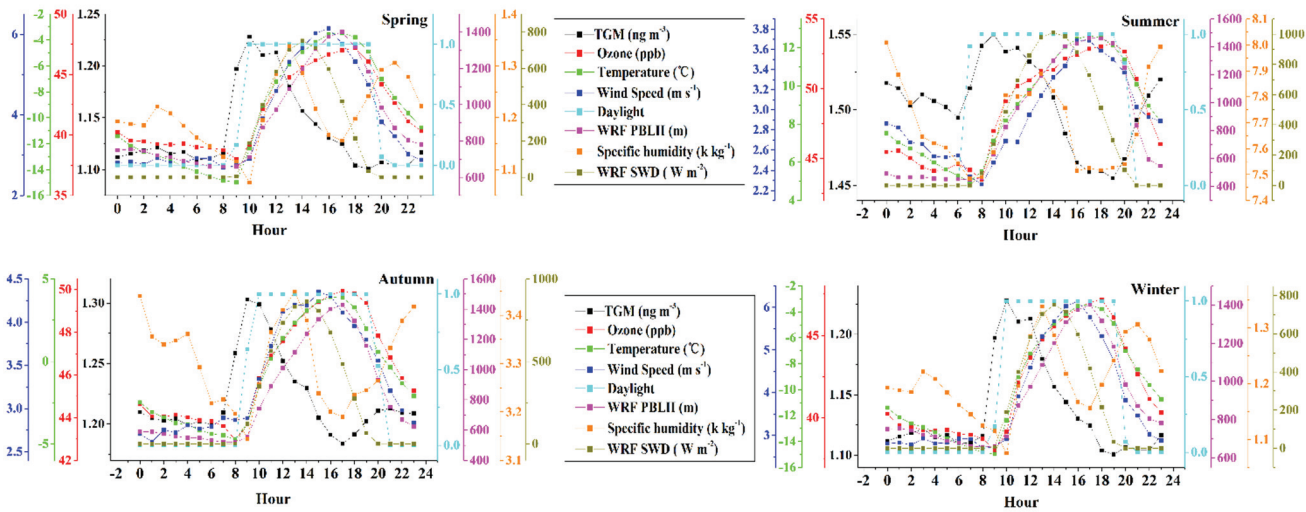
Fig. 8. Diurnal profiles of TGM, ozone and meteorological parameters (temperature, wind speed, daylight, WRF PBLH (planetary boundary layer height), specific humidity and WRF SWD (downward shortwave radiation)) at the Nam Co Station by seasons for the measurement period.

979

980
981 **Fig. 9. The measurements and Multi Linear Regression (MLR) model of TGM (top) and model residual (bottom) (residual =**
982 **measurement – simulation). The outliers are shown as circles.**
983
984
985
986
987
988
989
990
991
992
993
994
995
996
997
998
999
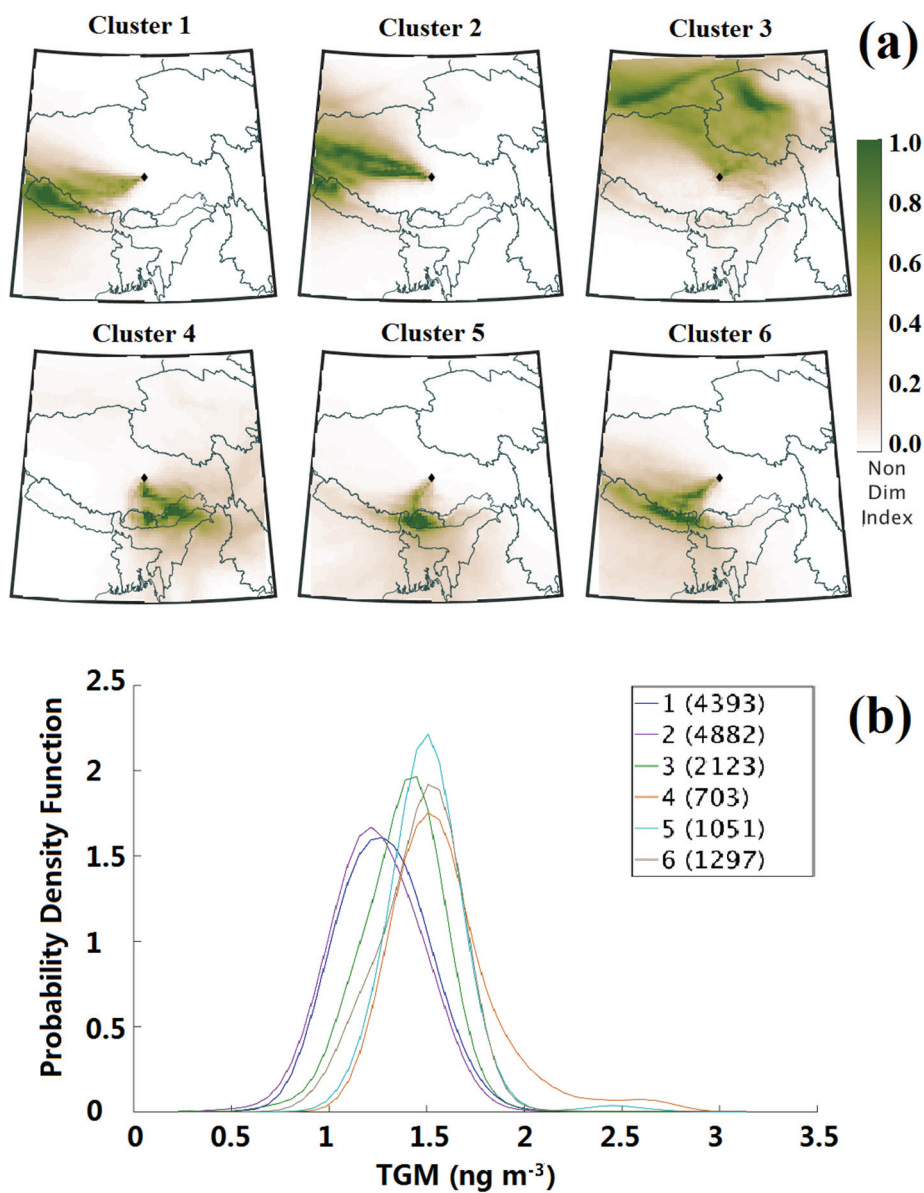
1002   **Fig. 10. Clusters of air mass transport to Nam Co using WRF-FLEXPART back-trajectories (a) and probability density function of**
1003   **TGM concentrations for each cluster, with number of data points in each cluster in parentheses (b).**

1004

1005

1006

1007

1008

1009 Fig. 11. Potential Source Contribution Function showing areas with possible emissions or air mass transport associated with higher
1010   TGM concentrations at the Nam Co Station by seasons in 2012.
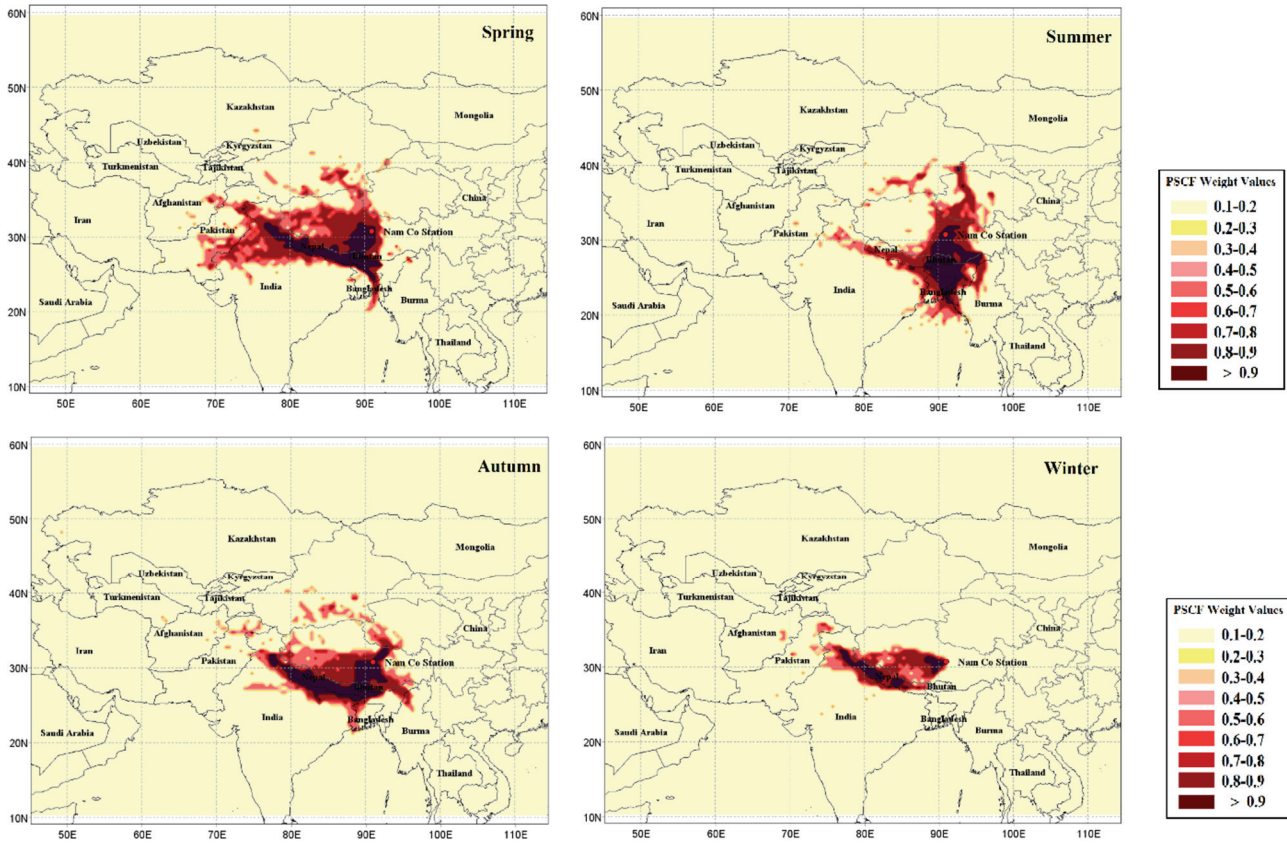
1011

1012

1013

1014

1015

1016

1017

1018

1019

1020

1021

1022

1023

TGM (ng m^{-3})
Sin fit of daily TGM (R^2 =0.42)
$y=1.29+0.21*sin(\pi*(x-108.15)/178.18)$

Temperature (℃)
Sin fit of daily T (R^2 =0.89)
$y= -0.83+10.77*sin(\pi*(x-111.11)/181.25)$

Relative Humidity (%)
Sin fit of daily RH (R^2 =0.37)
$y=51.12+14.43*sin(\pi*(x-89)/195.5)$

 Indian Monsoon Index
Sin fit of daily IMI (R^2 =0.67)
$y= -0.76+6.69*sin(\pi*(x-127.67)/182.58)$
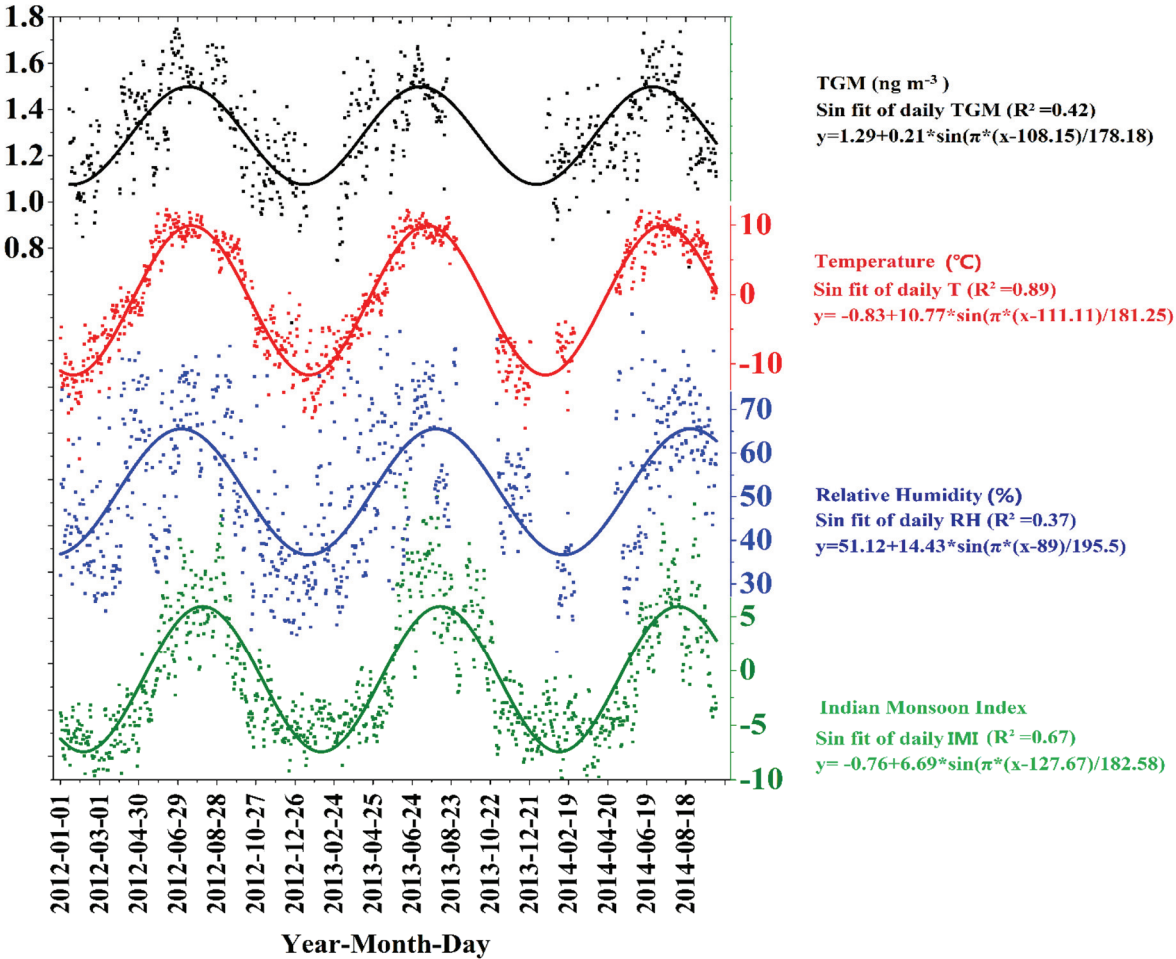
1024

1025

1026   **Fig. 12. Series of daily mean TGM, temperature, relative humidity and Indian Monsoon Index and their sinusoidal curve fits.**

1027

1028